Calhoun
Institutional Archive of the Naval Postgraduate School

Calhoun: The NPS Institutional Archive

DSpace Repository

Theses and Dissertations | 1. Thesis and Dissertation Collection, all items

2011-09

Measurements of the air-sea interface from an instrumented small buoy

Cheney, David J.

Monterey, California. Naval Postgraduate School

http://hdl.handle.net/10945/5502

This publication is a work of the U.S. Government as defined in Title 17, United States Code, Section 101. Copyright protection is not available for this work in the United States.

Downloaded from NPS Archive: Calhoun

http://www.nps.edu/library

Calhoun is the Naval Postgraduate School's public access digital repository for research materials and institutional publications created by the NPS community. Calhoun is named for Professor of Mathematics Guy K. Calhoun, NPS's first appointed -- and published -- scholarly author.

Dudley Knox Library / Naval Postgraduate School
411 Dyer Road / 1 University Circle
Monterey, California USA 93943

NAVAL POSTGRADUATE SCHOOL

MONTEREY, CALIFORNIA

THESIS

MEASUREMENTS OF THE AIR-SEA INTERFACE FROM AN INSTRUMENTED SMALL BUOY

by

David J. Cheney

September 2011

Thesis Advisor:	Qing Wang
Thesis Co-Advisor:	Thomas Herbers

Approved for public release; distribution is unlimited

THIS PAGE INTENTIONALLY LEFT BLANK

REPORT DOCUMENTATION PAGE		Form Approved OMB No. 0704–0188

Public reporting burden for this collection of information is estimated to average 1 hour per response, including the time for reviewing instruction, searching existing data sources, gathering and maintaining the data needed, and completing and reviewing the collection of information. Send comments regarding this burden estimate or any other aspect of this collection of information, including suggestions for reducing this burden, to Washington headquarters Services, Directorate for Information Operations and Reports, 1215 Jefferson Davis Highway, Suite 1204, Arlington, VA 22202–4302, and to the Office of Management and Budget, Paperwork Reduction Project (0704–0188) Washington DC 20503.

1. AGENCY USE ONLY *(Leave blank)*	2. REPORT DATE September 2011	3. REPORT TYPE AND DATES COVERED Master's Thesis

4. TITLE AND SUBTITLE Measurements of the Air-Sea Interface from an Instrumented Small Buoy	5. FUNDING NUMBERS
6. AUTHOR(S) David J. Cheney	
7. PERFORMING ORGANIZATION NAME(S) AND ADDRESS(ES) Naval Postgraduate School Monterey, CA 93943–5000	8. PERFORMING ORGANIZATION REPORT NUMBER
9. SPONSORING /MONITORING AGENCY NAME(S) AND ADDRESS(ES) N/A	10. SPONSORING/MONITORING AGENCY REPORT NUMBER

11. SUPPLEMENTARY NOTES The views expressed in this thesis are those of the author and do not reflect the official policy or position of the Department of Defense or the U.S. Government. IRB Protocol number NA.

12a. DISTRIBUTION / AVAILABILITY STATEMENT Approved for public release; distribution is unlimited	12b. DISTRIBUTION CODE

13. ABSTRACT (maximum 200 words)

An instrumented spar buoy, Met-on-a-Stick (MOAS), was designed, deployed, and validated for measuring the air sea interface processes at multiple levels. This system was deployed in June 2010 off the coast of California, and January and February 2011 in Monterey Bay. The system provides mean measurements of wind, temperature, and humidity at multiple levels within 3 m above the sea surface and measurements of sea surface temperature at three levels below ocean surface. It is small enough to be deployed and retrieved by two people. This thesis work introduces the design and the instrumentation of the system and evaluates the ability of the system for characterizing near-surface vertical variations of the marine boundary layer. The results indicate that the platform performance is as expected and is capable of providing measurements to characterize the fine variations close to the air-sea interface. We foresee a broad use of the MOAS in the future due to its low-cost and ease of deployment. Future improvements of the system include the use of better wind and GPS sensors to increase the quality of wind and wave measurements from the MOAS.

14. SUBJECT TERMS Air sea interaction, instrument buoy, air sea interface	15. NUMBER OF PAGES 77
	16. PRICE CODE

17. SECURITY CLASSIFICATION OF REPORT	18. SECURITY CLASSIFICATION OF THIS PAGE	19. SECURITY CLASSIFICATION OF ABSTRACT	20. LIMITATION OF ABSTRACT
Unclassified	Unclassified	Unclassified	UU

NSN 7540–01–280–5500

Standard Form 298 (Rev. 2–89)
Prescribed by ANSI Std. 239–18

THIS PAGE INTENTIONALLY LEFT BLANK

Approved for public release; distribution is unlimited

MEASUREMENTS OF THE AIR-SEA INTERFACE FROM AN INSTRUMENTED SMALL BUOY

David J. Cheney
Lieutenant Commander, United States Navy
B.A., Brigham Young University, 1999

Submitted in partial fulfillment of the
requirements for the degree of

MASTER OF SCIENCE IN METEOROLOGY AND OCEANOGRAPHY

from the

NAVAL POSTGRADUATE SCHOOL
September 2011

Author: David J. Cheney

Approved by: Qing Wang
Thesis Advisor

Thomas Herbers
Thesis Co-Advisor

Wendell Nuss
Chair, Department of Meteorology

THIS PAGE INTENTIONALLY LEFT BLANK

ABSTRACT

An instrumented spar buoy, Met-on-a-Stick (MOAS), was designed, deployed, and validated for measuring the air sea interface processes at multiple levels. This system was deployed in June 2010 off the coast of California, and January and February 2011 in Monterey Bay. The system provides mean measurements of wind, temperature, and humidity at multiple levels within 3 m above the sea surface and measurements of sea surface temperature at three levels below ocean surface. It is small enough to be deployed and retrieved by two people. This thesis work introduces the design and the instrumentation of the system and evaluates the ability of the system for characterizing near-surface vertical variations of the marine boundary layer. The results indicate that the platform performance is as expected and is capable of providing measurements to characterize the fine variations close to the air-sea interface. We foresee a broad use of the MOAS in the future due to its low-cost and ease of deployment. Future improvements of the system include the use of better wind and GPS sensors to increase the quality of wind and wave measurements from the MOAS.

THIS PAGE INTENTIONALLY LEFT BLANK

TABLE OF CONTENTS

I. INTRODUCTION....1
A. BACKGROUND....1
1. Monin-Obukhov Similarity Theory....1
2. Application of MOS....3
3. Air-Sea Interaction Involving Ocean Wave and Swell....4
4. Previous Development of Near Surface Measurement Platforms....5
5. High Resolution Air-Sea-Wave Interaction Project....5

II. MET-ON-A-STICK....7
A. SYSTEM DESIGN....7
1. Spar Buoy....9
2. HOBO Wind Speed Smart Sensor....10
3. HOBO 12-Bit Temperature Smart Sensor....10
4. Vaisala Radiosonde RS92....10
5. Genie GT 31/BGT-31....12
6. Temperature/RH Smart Sensor....12
7. HOBO Energy Logger....12
8. Setup....13
B. SYSTEM DEPLOYMENTS....14
1. June 18, 2010....15
2. June 20, 2010....15
3. June 24, 2010....15
4. January 21, 2011....16
5. February 2, 2011....16
6. February 3, 2011....17
C. DEPLOYMENT PROCESS....17
1. Preparation....17
2. Deployment....17
3. Retrieval....18
4. Post-processing....18
D. SENSOR EVALUATION....18
1. Temperature Sensor Intercomparison....19
2. Relative Humidity....23
3. GPS....27
4. Wind....30

III. DATA ANALYSIS....33
A. DATA OF INTEREST....33
1. June 2010....33
2. January 2011 Deployment....36
3. February 2011 Deployments....41
4. Flux Calculation....46

IV. CONCLUSIONS AND RECOMMENDATIONS 49
A. SUMMARY 49
B. RECOMMENDATIONS FOR FUTURE IMPROVEMENTS 50
LIST OF REFERENCES 53
INITIAL DISTRIBUTION LIST 57

LIST OF FIGURES

Figure 1. The MOAS deployed Feb 3, 2011. 8
Figure 2. Vaisala RS92 radiosonde (hydrometeoindustry.org 2011). 11
Figure 3. Deploying the MOAS on January 21, 2011 over the side of R/V John H. Martin....14
Figure 4. Comparison of the three temperature probes over a three-day period. The lines represent 1 to 1 comparison of temperature, while the top and bottom lines represent the variations from the center by ± 0.5° C. The temperature on the right in the legend is plotted on the x-axis. 19
Figure 5. Time series plot of temperature during calibration test of these sensors. This plot only spans a 1.5 hour time period during one of the higher temperature periods....20
Figure 6. Time series plot of temperature during calibration test of these sensors. This plot only spans a 1.5-hour time period during one of the lower temperature periods....21
Figure 7. Vertical variation and error range for temperature during the deployment on 2 Feb. 2011. The on standard deviation is based on 5-minute averages for each 2-minute period. 22
Figure 8. Vertical variation and error range for temperature during the deployment on February 2, 2011. The on standard deviation is based on 5-minute averages for each 2-minute period. This as the addition of the radiosonde data in black. 23
Figure 9. Relative humidity comparison with the three instruments all at the same height. The lines represent a 1 to 1 line with a ± 2% error bar. The relative humidity listed on the left in the legend is plotted on the X axis....24
Figure 10. Time series plot of relative humidity during calibration test. This period of 1.5 hours shows movement and differences in measurement. 25
Figure 11. Time series plot of relative humidity during calibration test. This period of 1.5 hours shows movement and differences in measurement. 25
Figure 12. Error plot of relative humidity with 5-minute averages and the standard deviation stepped every 2-minutes. This plot for the data from February 2, 2011....26
Figure 13. Relative Humidity error based the standard deviation on 5-minute averages every two minutes. This plot is for the data from February 2, 2011....26
Figure 14. Energy spectrum of GPS GT-31 attached to the Datawell buoy and the MOAS buoy and the NPS Datawell buoy from February 3, 2011 27
Figure 15. Energy spectrum of GPS GT-31 on the Datawell buoy and the MOAS buoy and the NPS Datawell buoy from February 3 2011. This figure shows a range between 0.05 – 0.3 Hz of the entire spectrum. 28
Figure 16. Significant wave height calculated from the entire energy spectrum for both February 2 and 3, 2011. 28

Figure 17. Significant wave height calculated from the 0.05—0.3 Hz part of the energy spectrum for February 2 and 3, 2011. 29
Figure 18. Water depth beneath the MOAS plotted from the initial location during February 2 and 3, 2011 deployments. The horizontal axis shows the range of travel from the initial deployment position. These data are derived from bathymetry of Monterey Bay, and the GPS position. 30
Figure 19. Wind data compared to each other. It is important to note that the variability is 1 m s^{-1}....31
Figure 20. Wind plots from February 3, 2011. Error bars calculated using the standard deviation of the data used to obtain the average wind speed. 32
Figure 21. Wind speeds for June 24, 2010, during HiRes2010, plotted as 30-minute running averages. 34
Figure 22. Sea temperatures measured on June 20, 2010, during HiRes2010. 35
Figure 23. Air/sea temperatures June 20, 2010 during HiRes2010. The radiosonde data is intermittent because the ship was in and out of range. 35
Figure 24. Air/sea temperatures January 21, 2011. The temperatures show the transition from unstable to stable thermal stability. 36
Figure 25. Air/sea temperatures January 21, 2011. This is the thermally unstable period of time. 37
Figure 26. Air/sea temperatures January 21, 2011. Shown here is the transition from thermally unstable to thermally stable stratifications. 37
Figure 27. Air/sea temperatures January 21, 2011. The temperatures show thermally stable stratification near the surface. 38
Figure 28. Sea temperatures measured on January 21, 2011. 38
Figure 29. Vertical wind profiles January 21, 2011, that show the calculated MOS profile using the top two of three measured levels. The different symbols showing the measurements at 1, 2, and 3 m correspond to thermally unstable (*), neutral (+), or stable (o). 39
Figure 30. Vertical potential temperature profile from January 21, 2011, calculated using MOS and the upper two measurement levels. The different symbols are used to indicate when the atmosphere is thermally unstable (*), neutral (+), or stable (o). 40
Figure 31. and specific humidity. 41
Figure 32. Vertical wind profile on February 3, 2011, showing the calculated MOS profile using the top and bottom of three measured levels (lines) and the measured wind (symbols). Different color/symbols denote results from a different time starting at 2140 and ending at 2320. Each profile represents an average profile from 30 minutes of measurements. 42
Figure 33. Vertical wind profile on February 2, 2011, showing the calculated MOS profile using the top two of three measured levels (lines) and the measured wind (symbols). Different color/symbols denote results from a different time starting at 2220 and ending at 2340. Each profile represents an average profile from 30 minutes of measurements. 43
Figure 34. Sea Temperatures averaged over one minute for February 2, 2011. 43
Figure 35. Temperature averaged over thirty minutes for February 2, 2011. 44

Figure 36. Sea temperatures averaged over 30 minutes on February 3, 2011. 45
Figure 37. Temperatures measured on February 3, 2011, showing a complete inversion of temperatures through the water and atmospheric layers.....45
Figure 38. Momentum flux calculated from data on January 21, 2011, using the top two levels of measurement.....46
Figure 39. Sensible heat flux (SHF) calculated from data on January 21, 2011, using the top two levels of measurement.....47
Figure 40. Latent heat flux (LHF) calculated from data on January 21, 2011, using the top two levels of measurement.....47

THIS PAGE INTENTIONALLY LEFT BLANK

LIST OF TABLES

Table 1. Summary of Specifications of Sensors Used on the MOAS. RS92 Refers to the Vaisala Radiosonde.....9
Table 2. Summary of Instruments' Altitude(s) for each Deployment. 13

THIS PAGE INTENTIONALLY LEFT BLANK

LIST OF ACRONYMS AND ABBREVIATIONS

ASIT	Air Sea Interaction Tower
ASIS	Air-sea Interaction Spar
CBLAST	Coupled Boundary Layers Air Sea Transfer
DNS	Direct Numerical Simulation
DRI	Departmental Research Initiative
Hi-Res	High-Resolution Air-Sea-Wave Interaction
LES	Large Eddy Simulation
LHF	Latent Heat Flux
MABL	Marine Atmospheric Boundary Layer
MOAS	Met on a Stick
MOS	Monin-Obukhov Similarity
ONR	Office of Naval Research
PRSWF	Phase-Resolved Surface Wave Field
RH	Relative Humidity
R/P FLIP	Research Platform Floating Instrument Platform
SHF	Sensible Heat Flux

THIS PAGE INTENTIONALLY LEFT BLANK

ACKNOWLEDGMENTS

I would like to express my heartfelt gratitude to my advisor, Dr. Qing Wang, for her guidance and instruction throughout the course of this research. Her dedication and wealth of knowledge has made this thesis a reality. I would like to offer my sincere gratitude to my co-advisor Dr. Thomas Herbers for his support, encouragement, and expertise. Without both of their help, this thesis would not be what it is today.

I would like to recognize Richard Lind in his design and countless hours of work and preparation that made the instrument what it is today and what it will be tomorrow. I would like to recognize Paul Jessen for his help throughout this study. His experience in working with the GPS and buoy data was invaluable.

It is also important to acknowledge the other professors at NPS who have inspired me and helped me reason through and apply the principles of meteorology and oceanography now and in the future.

It is important to acknowledge the crew of the R/V Robert Gordon Sproul, and to all those who participated in the ONR HIRES 2010 research project as well as the R/V John H. Martin and her crew for the class cruises for deployments in 2011. Their assistance deploying and recovering our buoys was an essential part of the success of our research.

Most importantly, I would like to thank my wife, Tira, and my six children, who supported me in my efforts to study, learn, and excel in all areas of my life while maintaining balance. I would be nothing without their support. I am grateful to my parents, who are always encouraging me to do my best. I would especially like to thank my Heavenly Father for His constant support and guidance.

THIS PAGE INTENTIONALLY LEFT BLANK

I. INTRODUCTION

A. BACKGROUND

Most measurements of the atmosphere over the ocean on buoys, ships or other platforms are set at a single level at 10 m or above. To obtain surface fluxes from such measurements, if the instrument is not at 10 m, it is adjusted to 10 m using the Monin-Obukhov Similarity Theory (MOS). However, the validity of MOS near the ocean surface in conditions of significant wind sea and swell has not been established because there have been limited observations of vertical profiles at the air-sea interface. A similar situation exists for near surface ocean temperatures, where it is measured just once at a single level (1 or 1.5 m of depth depending on the buoy, with ships measuring at the intake level for the engine room). As a result, phenomena occurring at the air-sea interface cannot be adequately identified and studied. The National Data Buoy Center provides the actual height of each buoy measurement, but the reported data is all converted to 10 m based on MOS.

The Met-on-a-Stick (MOAS) system is designed to measure the air/sea interface using in situ measurements with instruments that can measure the atmosphere and the ocean and show the interface structure. It is notable that the MOAS was designed to measure the lower few meters of the atmosphere as well as the top meter of the ocean at multiple levels. These measurements should allow us to evaluate the vertical variations of the wind, temperature, and moisture in comparison with MOS predicted vertical variations: and when MOS is applicable, calculate heat, moisture, and momentum flux at the surface.

1. Monin-Obukhov Similarity Theory

Similarity theory is based on the organization of variables into dimensionless groups, or the so-called dimensional analysis. As a result of dimensional analysis, we establish empirical relationships between groups of variables, also referred to as the non-dimensional groups. In the neutral atmospheric surface layer, defined as the lowest 10% of the neutral atmospheric boundary layer, non-dimensional analysis results in a

relationship between surface fluxes and the mean wind profile gradient, which can be integrated into the following:

$$\bar{u}(z) = \bar{u}(z_r) + \frac{u_*}{\kappa} \ln\left(\frac{z}{z_r}\right), \quad z_0 \le z \le h, \tag{1}$$

where $\bar{u}(z)$ is the mean wind at height z; z_r is a reference level within the surface layer; z_0 is the surface roughness length (or the depth of the roughness interfacial layer); u_* is the frictional velocity of the surface layer; and h_s is the height at the top of the surface layer. Equation (1) indicates that the mean wind in the surface layer varies with height logarithmically in neutral condition. This is the so-called 'log wind profile' of the neutral surface layer.

In non-neutral stability conditions, the flux-profile relationship is affected by thermal stability. Similar dimensional analysis results in a relationship that deviates from the log wind profile in Equation (1). The flux profile relationship can be generalized for all stability conditions as:

$$\bar{u}(z) - \bar{u}(z_r) = \frac{u_*}{\kappa} \int_{z_r}^{z} \phi_m\left(\frac{z}{L}\right) d\ln z$$

$$\bar{\theta}(z) - \bar{\theta}(z_r) = \frac{\theta_*}{\kappa} \int_{z_r}^{z} \phi_h\left(\frac{z}{L}\right) d\ln z \tag{2}$$

$$\bar{q}(z) - \bar{q}(z_r) = \frac{q_*}{\kappa} \int_{z_r}^{z} \phi_E\left(\frac{z}{L}\right) d\ln z$$

where L is the Monin-Obukhov length:

$$L = -\frac{u_*^3}{\kappa \frac{g}{\bar{\theta}} \overline{w'\theta'}} = \frac{u_*^3}{\kappa \frac{g}{\bar{\theta}} \theta_*}$$

θ_* and q_* are the temperature and specific humidity scales for the surface layer. The ϕ_m, ϕ_h and ϕ_E are empirical functions denoting the non-dimensional gradient of the surface

layer. The most frequently used ϕ functions are those derived from the 1968 Kansas experiment (Businger *et al.* 1971). In neutral conditions, Equation (2) will reduce to the log-wind profile in Equation (1).

2. Application of MOS

The profile relationship in Equations (1) and (2) describes the expected vertical wind, temperature, and specific humidity profiles with the given stability and how they are related to the surface layer turbulent fluxes. An important application of these relationships is that we can use profile measurements to derive surface fluxes when fast turbulence sampling is not available from direct flux measurements using the eddy correlation method. Specifically, if measurements from two levels are available, one can use these relationship to derive the 'star' variables, including u_*, θ_*, and q_* and hence obtain surface fluxes, which is the most frequent application of the MOS. In cases when only a single level of measurements is available, we define the surface roughness height (z_0) as the second known level where mean wind speed is assumed to be zero at the roughness height. Over the ocean, the roughness height is related to surface wind stress to describe the effect of wind driven waves (Charnock 1955), while the air temperature at z_0 is assumed to be the same as the sea surface temperature (SST). For moisture at z_0, we normally assume saturation at the SST. Bulk aerodynamic formulation is the most frequently used surface flux parameterization in global and regional forecast models. It was originally derived from the flux-profile relationship based on the MOS theory. If the results of MOS theory are in question, one needs to have a serious look at the bulk aerodynamic formulation as well.

Another application of the MOS theory is to obtain mean wind, temperature, and humidity at an altitude without direct measurements. This is especially important to the application of the bulk aerodynamic formulation that calls for mean quantities at 10 m height; whereas, most measurements are made at a different level.

3. Air-Sea Interaction Involving Ocean Wave and Swell

The basic assumption of MOS is that the boundary layer is in equilibrium with the underlying surface and that the turbulent field is horizontally homogeneous. These assumptions in many cases are violated over the ocean as winds and waves in marine boundary layers are often in an unsettled state when fast-running swell generated by distant storms propagates into local regions and modifies the overlying turbulent fields. Some of the past field experiments, such as the Coupled Boundary Layers Air-sea Transfer (CBLAST low wind) field campaign (Edson et al. 2007), are focused on non-equilibrium, the variable nature of winds, and waves at low winds. Sullivan et al. (2008) showed the average drag coefficient (C_D) varied linearly with wind speed in close agreement with the Tropical Ocean and Global Atmosphere Coupled Ocean–Atmosphere Response Experiment (TOGA COARE) 3.0 parameterization (Fairall et al. 2003). However, there was large scatter in C_D at low wind speed. Moreover, over certain periods, $C_D < 0$, suggests a low-level wind reversal. Sullivan et al. (2008) hypothesized that some of the scatter in C_D is attributed to the non-equilibrium state of winds and waves at low winds. Miller (1998) showed the time series of surface layer winds collected from the Research Platform Floating Instrument Platform (R/P FLIP). It clearly showed the hourly transition from a logarithmic to nearly uniform, near-surface wind profile after a storm passage; coincident with the wind-profile change is a rapid reduction in the turbulent momentum flux. These features appear to be signatures of a wave-driven surface layer and invalidate the use of Monin–Obukhov Similarity Theory that often is used to predict air-sea fluxes (Rutgersson et al. 2001). However, the overall impact of waves and swell and its vertical extent is not fully understood. Measurements of the lower surface layer in various conditions are needed to fully understand the mechanism of air-sea interaction involving waves and swell.

There are very few observations in this vertical area of the atmosphere near the interface, which include the ocean at multiple levels, allowing for study of these physical parameters. Part of our purpose is to gain further observations near the interface in various boundary layer and wave conditions, which contribute to better understanding of the air-sea coupling processes to eventually help improve model parameterization.

4. Previous Development of Near Surface Measurement Platforms

Many previous measurements have attempted to sample the vertical variation of wind, temperature, water vapor and turbulence near the air-sea interface. Many of these efforts were carried out from stabilized platforms such as the Research Platform Floating Instrument Platform (R/P FLIP, Miller 1998), or the Air-sea Interaction Tower (ASIT, Edson et al. 2007). Research buoys are an alternative to the stabilized platforms. One such buoy is the Air-sea Interaction Spar (ASIS) that was designed and tested for measurement on both sides of the air-sea interface (Graber et al. 1999). ASIS is able to measure both mean profiles at several levels and turbulence at a single level. Its instruments span the bottom 5 m of the atmosphere at four different levels. It has a very large power requirement, which requires it to be tethered, and it is very difficult to deploy at a length of 11 m (Graber et al. 1999). To sample the air-sea interface in various conditions, a simple and easily deployable system is needed although it may be at the expense of instruments for direct turbulence measurements due to power and weight constraints. This is the motivation for developing the met-on-a-stick. Our intention was to design and test a system that can be deployed from any platform with minimal power requirements.

5. High Resolution Air-Sea-Wave Interaction Project

This thesis work is part of the NPS efforts within the High-Resolution Air-sea–Wave Interaction (Hi-Res) Departmental Research Initiative (DRI) sponsored by the Office of Naval Research (ONR). The practical objectives motivating the establishment of the Hi-Res are the determination of how well ship-based radars can measure the phase-resolved surface wave field (PRSWF), testing the skill of highly-nonlinear numerical surface wave models to predict the evolution of the PRSWF, and the incorporation of ocean wave effects into models of the Marine Atmospheric Boundary Layer (MABL). Together, enhanced skills in these areas would lead to the goal of improved predictions of the PRSWF around surface vessels and would contribute to the safety and effectiveness of naval operations in moderate to high wind and sea states. While these are practical objectives and goals, their achievement will stretch the scientific limits of wind and wave

measurements, theory and modeling, and our understanding of microwave (radar) scattering at grazing incidence. The ultimate goal of the program is to develop the basis for the next generation of large eddy simulation/direct numerical simulation (LES/DNS) models of the coupling between the ocean-wave-atmosphere systems, which will need to have wave-resolved dynamics and kinematics. In order to achieve its goals the DRI included field measurements, theory, and numerical modeling of the wind-wave interaction problem.

Hi-Res field measurements were conducted in two phases: a pilot experiment in June 2009 (Hi-Res2009) and a full field intensive observation period in June of 2010 (Hi-Res2010). Hi-Res2009 was conducted in weak wind conditions, while Hi-Res2010 was conducted west of Bodega Bay, CA about 40 km away from the coast. The major measurement platforms involved in Hi-Res included R/P FLIP, a stabilized research vessel fully equipped for near-sear face atmospheric and oceanic measurements, and a research vessel, R/V Robert Gordon Sproul with similar instrumentation.

The NPS Meteorology instrument suite was deployed on the R/V Sproul in both 2009 and 2010. The basic instruments included one or two flux measurement towers, a radiosonde sounding system, a wind sampling sodar, and a laser ceilometer. In addition to these fixed location measurements, the NPS team also experimented with measurements from a small free floating instrumented spar buoy for near surface gradient sampling in both the atmosphere and the ocean. This buoy is referred to as the met-on-a-stick, or the MOAS. This thesis work focused on evaluating the performance of the MOAS for air-sea interaction studies.

II. MET-ON-A-STICK

The instrumented small buoy, Met-on-a-Stick (MOAS), was developed at NPS in order to measure the air-sea interface. It was deployed as part of the Hi-Res2010 experiment and on subsequent deployments in conjunction with various at-sea cruise courses to determine its capabilities and weaknesses in measuring the layers near the air-sea interface. Here we will discuss the design and instrumentation in detail and determine its inadequacies in order to further improve the system.

A. SYSTEM DESIGN

The MOAS is intended to characterize the air-sea interface without significant disturbance to the atmosphere and ocean. The objective is to design a small and easily deployable system that can adequately sample more than one level in the atmosphere and in the ocean. Some measure of the surface waves is also desirable. A prototype of the MOAS was deployed in Hi-Res2009 on a small spar buoy owned by Scripps Institution of Oceanography at the University of California, San Diego. The system was deployed in Hi-Res2010 with instruments mounted on a small spar buoy with a radar reflector on top. In January and February 2011, a further modified the MOAS was again tested during a few short cruises on the R/V John H. Martin. In this chapter, we will discuss the general system design and the sensor properties used in the final phase of the MOAS that were tested during the post-Hi-Res cruise on the R/V John H. Martin.

The basic requirement for the MOAS was to obtain the vertical gradient of thermodynamic properties and wind for the bottom few meters of the atmosphere and the water temperature gradient at the top meter of the ocean. Such measurements would provide a vertical profile of the measured quantities. We added a GPS sensor later to investigate the relationship between wind and ocean wave heights. We also added a radiosonde to obtain an additional level of temperature and humidity measurements, as well as pressure and the GPS location of the buoy. A picture of this system deployed on February 3. 2011 is shown in Figure 1. In this configuration, the anemometers are located at three levels together with the temperature and humidity sensors inside radiation shields

at each level. The radiosonde is taped to the top of the mast and the GPS receiver can be seen on the right side of the float. A summary of sensor resolution and accuracy is given in Table 1. We will explore each of these individually and identify their use in this experiment.

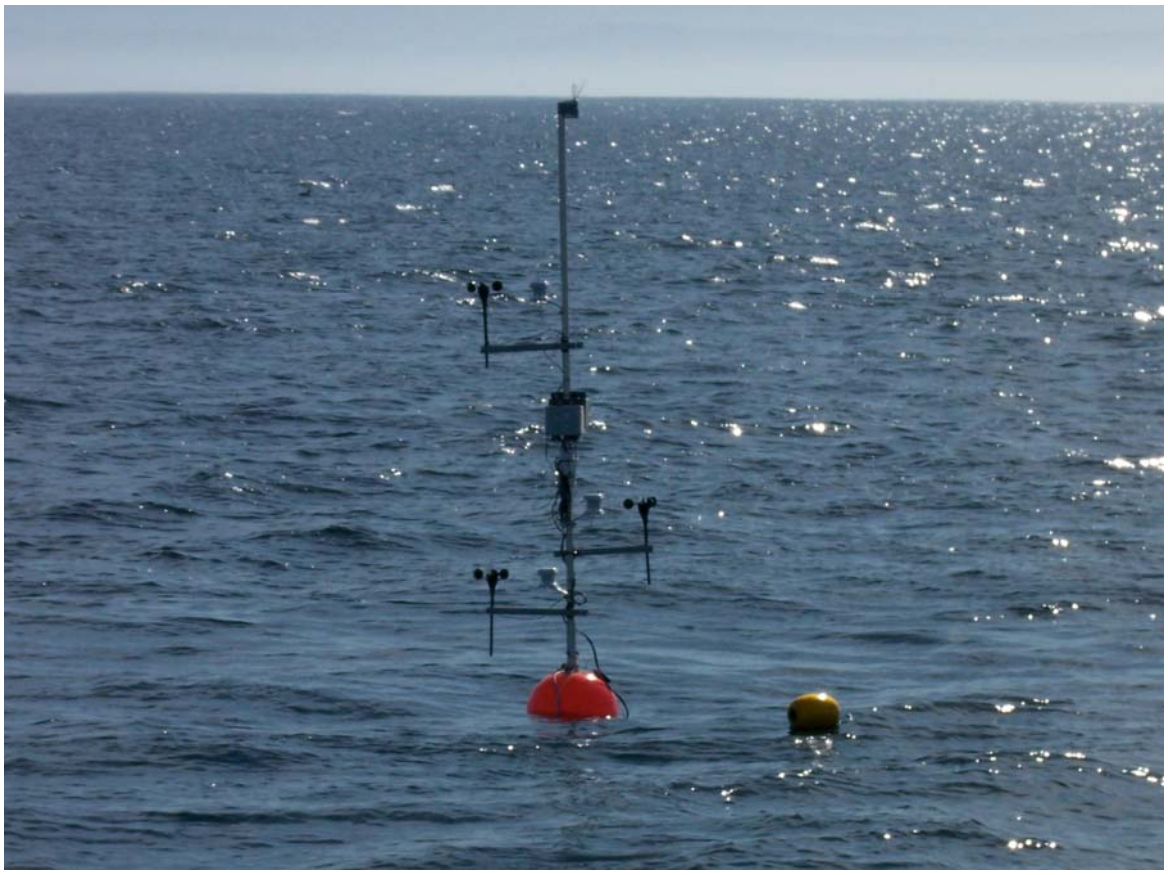

Figure 1. The MOAS deployed Feb 3, 2011.

Table 1. Summary of Specifications of Sensors Used on the MOAS. RS92 Refers to the Vaisala Radiosonde.

Sensor	Range	Resolution	Accuracy
Wind	1–54 m s^{-1}	0.38 m s^{-1}	1.1 m s^{-1}
Temperature	-40°C–100°C	0.03 °C	0.2 °C
Temperature/RH	-40°C–75°C 0% – 100%	0.02 °C @ 25°C 0.1 % @ 25°C	0.21 °C 2.5%
RS92 Temperature **RH** **Pressure**	-90 °C –60 °C. 0% – 100% 1080 hPa – 3 hPa	0.1 °C 1% 0.1 hPa	0.15 °C 2% 0.4 hPa

1. Spar Buoy

The decision to place all of this equipment on a spar buoy was to make it possible to deploy multiple instruments without significant changes in horizontal position due to leaning or tilting. With the 15 kg weight 3 m below the water line, much of the tilting and tipping that could occur would be greatly minimized with a balanced weight in the water column. We used two different spar buoys with a similar system setup during Hi-Res2010 and during the post-Hi-Res2010 R/V Martin cruise. The one used in the Hi-Res2010 experiment was a float with a radar reflector on top used by another group to identify the location of small buoys. This radar reflector was taken off for the last deployment in Hi-Res2010. It was determined that the radar reflector on top of the small buoy maybe a source of excessive drag causing the buoy to lean over from the wind. We decided to purchase a similar buoy without the reflector. The 19”spar buoy (BB60, 19”) made by the SNL Corporation was selected to be used for the final set-up of the MOAS.

The SNL spar buoy has a total length of 6 m with 3 m above the water line. The bare buoy weighs about 25 kilograms. Fully loaded with sensors, the buoy can be

deployed from a small boat by two people. All instruments described below are attached to the spar buoy using various methods, enabling exact placement of each.

2. HOBO Wind Speed Smart Sensor

Wind sensors were placed at three levels to characterize the vertical variation of the wind. The 3-cup anemometer sensor is a plug-in HOBO weather station wind sensor. It measures wind speed from 0–45 m s^{-1} with a resolution of 0.38 m s^{1}. Its starting threshold is 1 m s^{-1} (Onset 2011b). The first deployment of the MOAS during Hi-Res2010 did not have wind sensors attached. These were added to the second deployment replacing the temperature and humidity sensors. In most of the deployments, the wind sensors were at 1, 2, and 3 m, but they can be placed at nearly any level along the length of the buoy.

3. HOBO 12-Bit Temperature Smart Sensor

These temperature sensors were used for measuring the water temperature. We attached them to a line, nominally placing them at: -0.1 m, -0.3 m, and -0.6 m. The line was also fitted with a float for the surface and a weight on the end of the line, to keep the sensors at specific depths. Temperature sensors measure from -40 °C to 100 °C with a resolution of 0.03 °C (MicroDAQ.com 2011c). No protections were added to these instruments since they were used in the water.

4. Vaisala Radiosonde RS92

We added a radiosonde (Figure 2) to replace one of the temperature/humidity sensors. We were able to use it to track position and get real-time data when the ship was in range. The radiosonde was placed at differing levels based on need or space for that deployment. It added another level of humidity and temperature, as well as pressure and GPS positioning. The radiosonde uses GPS measurements to determine wind speed and direction by tracking its movements. With the radiosonde strapped to the pole, wind cannot be measured however mean drift speed and direction of the MOAS was derived from these measurements. The temperature sensors resolution is 0.1 °C with a range of -90 °C to +60 °C. The response time is less than 0.4 s for the surface. The humidity sensor

resolution is 1% relative humidity (RH) with a range from 0% RH to 100%RH. The RH response time is less than 0.5 s for near the surface. The pressure resolution is 0.1 hPa with a range of 3 hPa to 1080 hPa (Vaisala 2011). We attached the radiosonde using duct tape.

Figure 2. Vaisala RS92 radiosonde (hydrometeoindustry.org 2011).

5. Genie GT 31/BGT-31

This GPS navigator was added in an attempt to test the capability of the MOAS in measuring surface waves simultaneously with other variables for better characterization of the air-sea interaction processes. Professor Thomas Herbers' research group, in the Oceanography Department of the Naval Postgraduate School tested this same sensor to determine its ability to measure significant wave height. It is a compact hand held GPS receiver, which is intended for use in navigation both over the water and on the land. It is waterproof and floats if dropped in the water. It can also be used as a GPS data logger with a stay time of up to 41 hours in normal mode (Locosys 2007). The BGT model adds Bluetooth capability, reducing operation time to 33 hours. The GT-31 operates at frequency L1 1575.42 MHz and updates at 1Hz. The antenna is a built-in patch antenna. These GPS units use Space Based Augmentation Systems (SBAS) (Locosys Technology 2009), a technique based on a differential GPS that makes the measurements more accurate, better than 1 meter for higher accuracy GPS receivers (SX Blue GPS Series 2011).

6. Temperature/RH Smart Sensor

Temperature and relative humidity (RH) sensors were used at three levels; generally, 1, 2, and 3 m. The sensors have a temperature range of -40 °C to 75 °C with a resolution of 0.02 °C and having the full humidity range with 0.1% RH resolution. The response time is 5 minutes for both (MicroDAQ.com 2011a). This sensor requires protection from rain or direct splashing. Two of the sensors failed after being exposed to sea spray. It was used with the radiation shield RS3, which is also a HOBO product.

7. HOBO Energy Logger

The HOBO Energy Logger was used as the data acquisition system on the MOAS. The logger automatically recognizes each sensor type and serial number. The logger is programmed and initialized when connected to a computer that has the HOBOware software installed. Once set up, the logger will be in standby until started by pressing the start button. It has 512K of memory and a battery life of about one year

(Onset 2011a). The sensor determines the order of display for data by serial number on each device. Hence, it does not matter which slot the sensor is plugged into.

8. Setup

The wind sensors and temperature/RH sensors are attached to the buoy pole using brackets. The radiosonde was attached using duct tape. The GPS unit was attached using Velcro to the buoy float, and the water temperature sensors were attached using a cord that tied onto the buoy and had a float and weight attached. This line would float several feet from the buoy.

Sensors and sensor locations on the MOAS varied during the several testing deployments of the MOAS on various research vessels. Table 2 gives a summary of sensors height above water during each deployment. It is discussed in more detail in the next section.

Table 2. Summary of Instrument Altitude(s) for each Deployment.

Deployment date	**Sensors**	**Level**
18 June 2010	Temperature/RH Water temperature	1m, 3m -0.1m, -0.3m, -0.6m
20 June 2010	Temperature/RH Water temperature RS92	1m, 3m -0.1m, -0.3m, -0.6m 2m
24 June 2010	Wind Water temperature RS92	1m, 2m, 3m -0.1m, -0.3m, -0.6m 2m
21 January 2011	Temperature/RH Water temperature Wind	1m, 2m, 3m -0.1m, -0.3m, -0.6m 1m, 2m, 3m
02 February 2011	Temperature/RH	1m, 2m, 3m

	Water temperature	-0.1m, -0.3m, -0.6m
	Wind	1m, 2m, 3m
	RS92	2.6m
	BGT-31	On buoy float
03 February 2011	Temperature/RH	0.6m, 1m, 2m
	Water temperature	-0.1m, -0.3m, -0.6m
	Wind	0.6m, 1m, 2m
	RS92	2.8m
	BGT-31	On buoy float

B. SYSTEM DEPLOYMENTS

During the testing stage of the MOAS, several deployments took place with different positions (Table 2) and from different platforms. A picture of the test deployment from the R/V Martin is shown in Figure 3.

Figure 3. Deploying the MOAS on January 21, 2011 over the side of R/V John H. Martin

1. June 18, 2010

This first deployment in June 3010 was during the HiRes2010 experiment off the coast of Northern California conducted from the R/V Sproul. We first deployed the buoy off the stern while at anchor to verify that the buoy would perform as expected. We were able to show that the buoy would stand upright and that we could get it on and off the boat. We logged a short period of data to test the data acquisition system. Because the buoy was tethered to the ship, the data were not used for analysis.

2. June 20, 2010

June 20 was the first time deploying the MOAS from the ship in rough seas. The deployment was a success in the sense that all atmospheric sensors stayed above water and everything went overboard without getting tangled. For this deployment, we had temperature and humidity sensors at 1 m and 3 m with a radiosonde attached at 2 m. The sea temperature sensors were also attached to the buoy. A radar reflector was installed at the top. Only one data logger was used, so we were limited to sampling from six instruments. The 2-meter temperature/humidity sensor had failed prior to deployment. The buoy was in the water for nearly two hours. During this time the bottom temperature/humidity sensor failed, and we received only some data from the radiosonde. We learned that we needed to be close to the buoy to keep contact with the radiosonde. For this deployment with about 10-foot seas, so we lost contact with the radiosonde at about 1 km. The radar reflector and the method of attaching retrieval line with a float added drag to the MOAS during this first deployment, resulting in noticeable (~10 degree) constant tilt.

3. June 24, 2010

On our second deployment, all temperature/humidity sensors had failed prior to deployment. They were replaced with wind sensors at 1, 2, and 3 m. The water temperature sensors were deployed each time without instrument issues. The radar reflector was taken off to minimize wind drag. The float line was moved to above the water line to also minimize drag. A radiosonde was strapped to the stick at the same level as before. The buoy was deployed for about three hours. Once again, the radiosonde

telemetry was lost as the ship went out of range. With the wind sensors all in a row, we assumed that the buoy would align itself into the wind. This was not the case, however, and the buoy spun around in circles, wrapping the water temperature sensors around the buoy. This introduced uncertainty about the measurement levels of the water temperature sensors. With the removal of the radar reflector and repositioning of the float line, the MOAS rode nearly vertical during this deployment.

4. January 21, 2011

This deployment of the MOAS from the R/V John H. Martin in the Monterey Bay was part of the cruise for the Tactical Oceanography class at NPS. We were deployed for most of the day leaving from the Monterey Coast Guard pier. This is the first time we used the SNL buoy. We added a rudder under the water by clamping a plastic lid from a container to the pole. This prevented the buoy from spinning around in circles. We tied the lead line to the buoy using a rope above and below the float so it would not pull on the top or bottom of the buoy unevenly. Temperature/humidity sensors and wind sensors were included at 1, 2, and 3 m. We added another data logger for the extra sensors, with the above-water sensors feeding one and the sea temperature sensors feeding the other. This deployment had our system moored for 6 hours as part of another experiment. The sensor stood upright in the water with no indication of tilting, even when going over waves. The sea temperature sensors did not wrap around the pole as in the previous deployment. Seas were smooth with just a long period swell of less than 1 m, and the winds less than 5 m s^{-1}.

5. February 2, 2011

We were again on the R/V John H. Martin in the Monterey Bay, this time as part of the Wave and Surf Forecasting class. We deployed in the early afternoon out of Moss Landing. We used the same set up as the last deployment with the addition of a radiosonde strapped to the MOAS buoy at 2.6 m and the BGT-31 GPS receiver attached to the buoy for this deployment. As part of the class cruise, there were two NPS Datawell buoys deployed with the GT-31 GPS receivers attached. This deployment lasted about two hours, and had low wind with swell conditions of 1 m with winds less than 5 m s^{-1}.

6. February 3, 2011

The MOAS was again deployed with the Wave and Surf class in the Monterey Bay on board the R/V John H. Martin. We adjusted the levels of the sensors from the previous day to have wind temperature and humidity sensors located at 0.6, 1, and 2 m with the radiosonde at 2.8 m. We still deployed the GPS both on the MOAS buoy as well as on the NPS Datawell buoys. The swell conditions were higher on this day at 1.5 m with the winds still less than 5 m s^{-1}.

C. DEPLOYMENT PROCESS

1. Preparation

The MOAS took some time to put together with all of the sensors that are being attached. This initially took several hours to attach all of the instruments to the pole and get the wires all strapped down securely and attached to the data loggers, which were placed in waterproof boxes. Subsequent deployments did not require set up time unless the sensors were being moved. Once all of the instruments are installed, they must be initiated by attaching the data logger to a computer with the software program to start the logging process. This can be done anytime before the deployment. For the deployment on 21 January, we did this the day before, so it was ready to go the next morning. The logger waits until the "start" button is pressed to begin logging data. Immediately before deployment, the box must be opened and the button pressed. This process always gives some data before the instrument is in the water.

When using the radiosonde, there are antennas, a receiver/processor, and another computer, which must be dedicated to its use. The radiosonde is initiated while linked to the computer and strapped to the pole just before deployment.

2. Deployment

The buoy can be stored in three pieces. Once the buoy is put together, the entire system is about 6 m long. Once the GPS unit is attached to the buoy, the radiosonde is initialized and strapped on, and the data loggers are started, and the MOAS is ready to be deployed. The water temperature sensors are attached to a rope that allows some space

between the pole and the sensors. Care was taken to avoid getting them tangled during deployment. The rope is long enough to put the stick over board and then throw in the water sensors. Two people are required to get it over safely. The weighted end is dropped in and then the pole is lowered until the buoy is in the water. While the system is deployed, data from an attached radiosonde can be viewed if the ship is in range. Data from the HOBO sensors cannot be viewed in real time.

3. Retrieval

For retrieving the MOAS, the ship needs to be close enough to the buoy to so that someone on the ship can grab the top of it. Sometimes we were able to drive right up next to it. Sometimes we needed to use a pole or a grappling hook to bring it closer. Lifting the buoy from the top is a little difficult, and the instruments could easily be broken off at this point. With it part way out of the water, a second person can help lift the bottom out of the water.

4. Post-processing

The data from the GPS can be downloaded from the SD card that is inside it or it can be attached to a computer to retrieve the data. The data are in a format that is not immediately recognizable, and must be processed by a program that recognizes the format. In order to retrieve the desired wave data, we used a program in MATLAB written by Paul Jessen, who is experienced in processing the GT-31 data.

The HOBO loggers with the HOBOware software have several options for data output including comma-separated values and into Excel. The data from the radiosonde can also be placed in comma-separated values format from the Vaisala program used to retrieve the data while it is deployed. All data was imported into MATLAB for analyses.

D. SENSOR EVALUATION

Consistency among sensors at different levels is important for the MOAS measurements as the measured gradient of wind and thermodynamic properties are of more importance than the variable itself. As a result, the sensors need to be calibrated against each other to avoid systematic bias. This effort has been done in a couple of ways.

For the instruments that were measuring meteorological data, we designed a test experiment that would allow them to measure simultaneously at the same location. The anemometers and the HOBO temperature and RH sensors were placed at the same level off the ground away from obstructions for three days.

1. Temperature Sensor Intercomparison

Measurements from the three HOBO temperatures from the test experiment are plotted against each other in Figure 4. This figure shows that all three temperature sensors follow each other well. In the middle range between 10 and 16 °C, temperature at the second level seems to be biased toward the lower values by about -0.1 °C. The average bias from the other two sensors is about 0.02 °C. There is clearly some variability as the sensors respond to changing conditions.

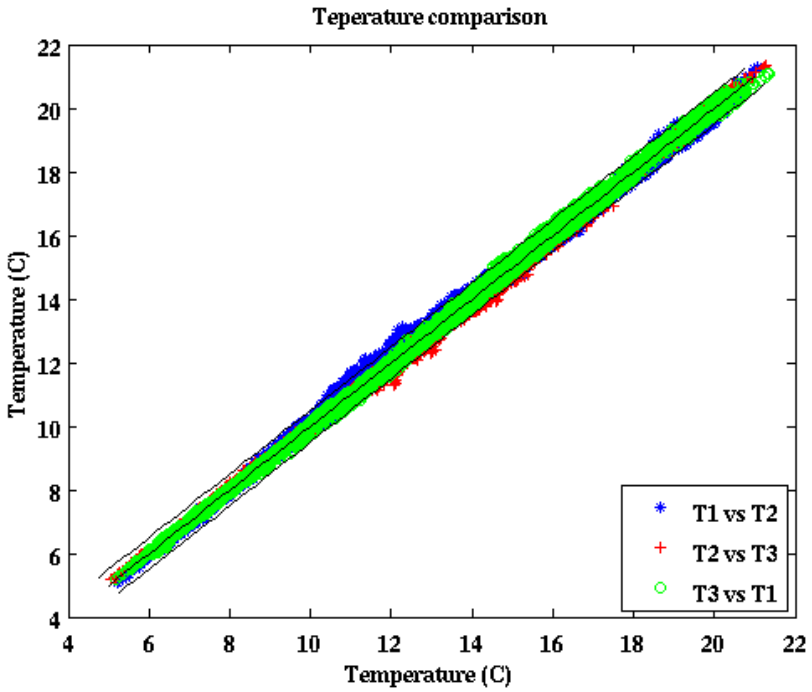

Figure 4. Comparison of the three temperature probes over a three-day period. The lines represent 1 to 1 comparison of temperature, while the top and bottom lines represent the variations from the center by ± 0.5° C. The temperature on the right in the legend is plotted on the x-axis.

Figures 5 and 6 show the time series of all three atmospheric temperature sensors on the MOAS. The HOBO temperature probes follow each other rather closely, although temperature from level 1 seems to overestimate at times compared to those from the other two levels. In these two plots we show that even though there is a difference from one sensor to another, this difference is not constant, and could be measuring real atmospheric differences. Since the intention of the MOAS is to characterize the vertical gradient of the mean vertical profiles of wind, temperature, and humidity, it is important that the error between sensors at different levels is identified.

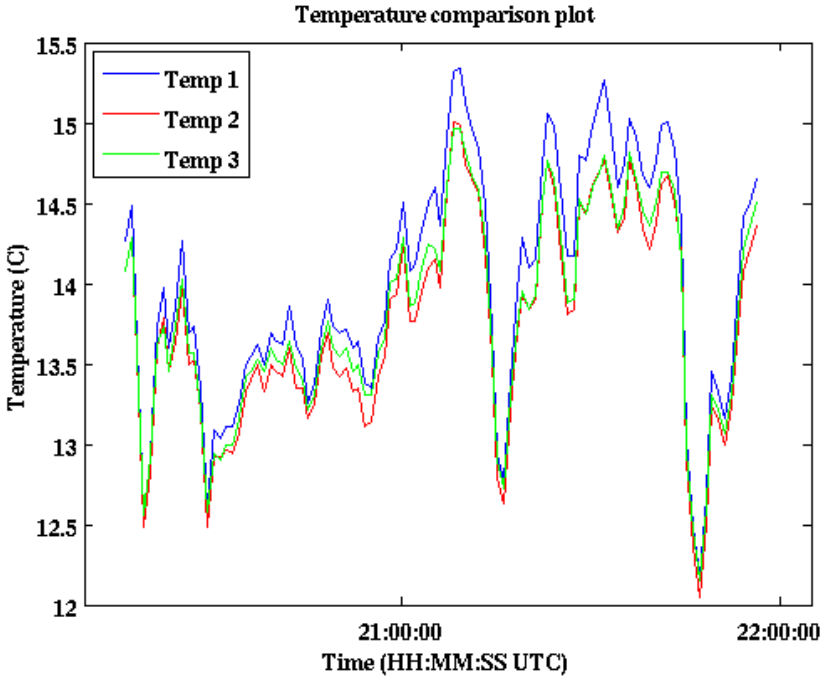

Figure 5. Time series plot of temperature during calibration test of these sensors. This plot only spans a 1.5 hour time period during one of the higher temperature periods.

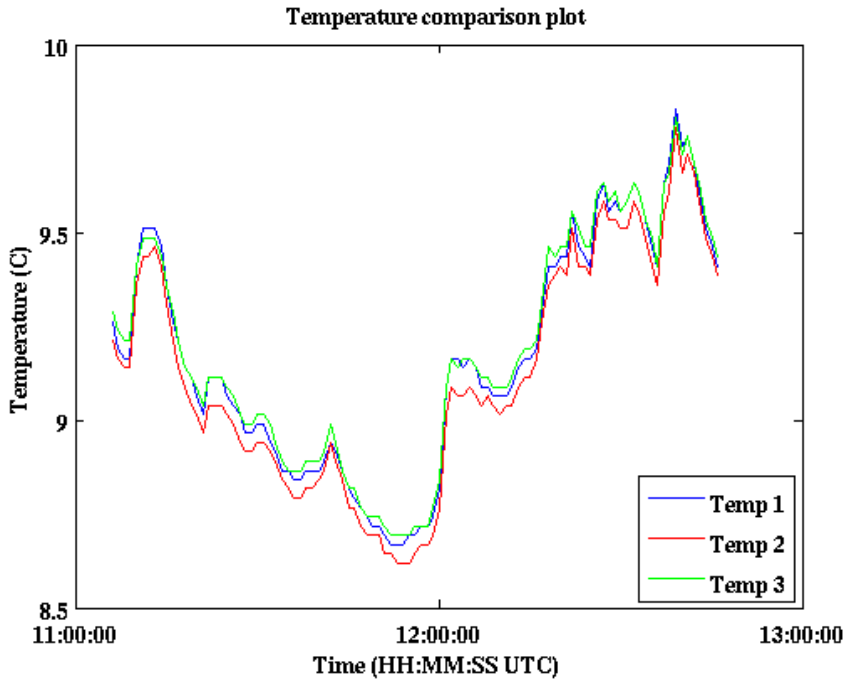

Figure 6. Time series plot of temperature during calibration test of these sensors. This plot only spans a 1.5-hour time period during one of the lower temperature periods.

We examined the mean and variance of the measurements at each level before discussing any gradients seen in the field measurements. An example of such analyses is shown in Figure 7, where the measurements were made on 2 February 2011. Here we took the originally sampled data and performed a five-minute running average with a time step of two minutes. In this way there is overlap of the data ensuring that each data point is used and accounted for. We calculated the standard deviation of the data and plotted standard deviation as error bars. If one assumes Gaussian distribution for the measured temperature, about 68% of the samples should lie between the two ends of the error bars. Figure 7 shows minimal overlap of the average data and the range of temperature covered by its corresponding error bars from each level. This indicates that the difference in the measured data from the three levels is statistically different.

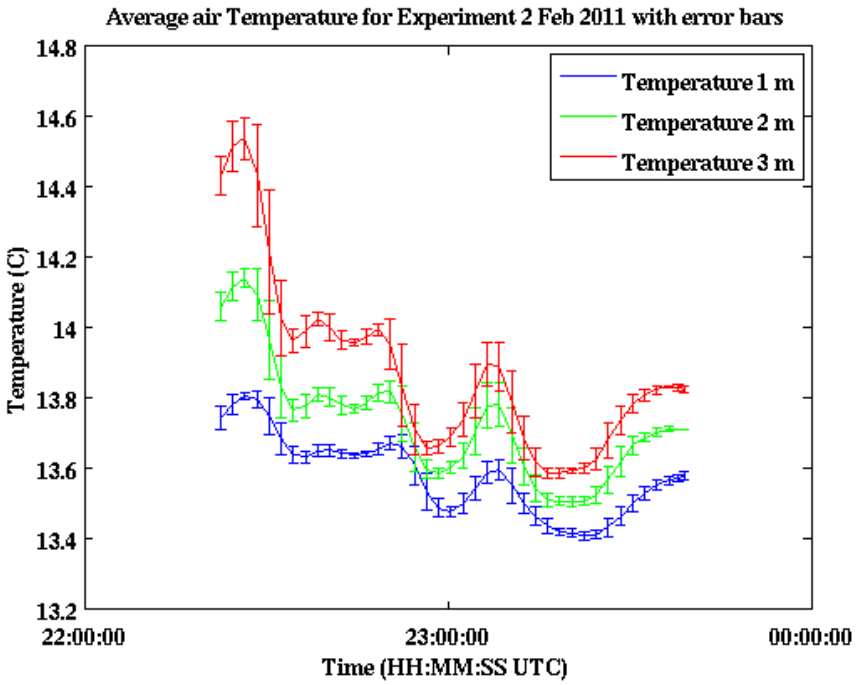

Figure 7. Vertical variation and error range for temperature during the deployment on 2 Feb. 2011. The on standard deviation is based on 5-minute averages for each 2-minute period.

The Vaisala RS92 radiosonde was strapped to the pole of the MOAS for an additional temperature and humidity measurement. In Figure 8, the variation of the RS92 temperature is shown together with those shown in Figure 7. Notice that the radiosonde data had more significant variability compared to the HOBO sensors. Although the addition of the RS92 added another level of data, it does not compare well with the HOBO data. This may result from the different response of the sensors, some degree of solar heating in the light winds, or internal processing of the radiosonde system. If one intends to identify vertical variations with multiple levels, it is not beneficial to use completely different types of sensors.

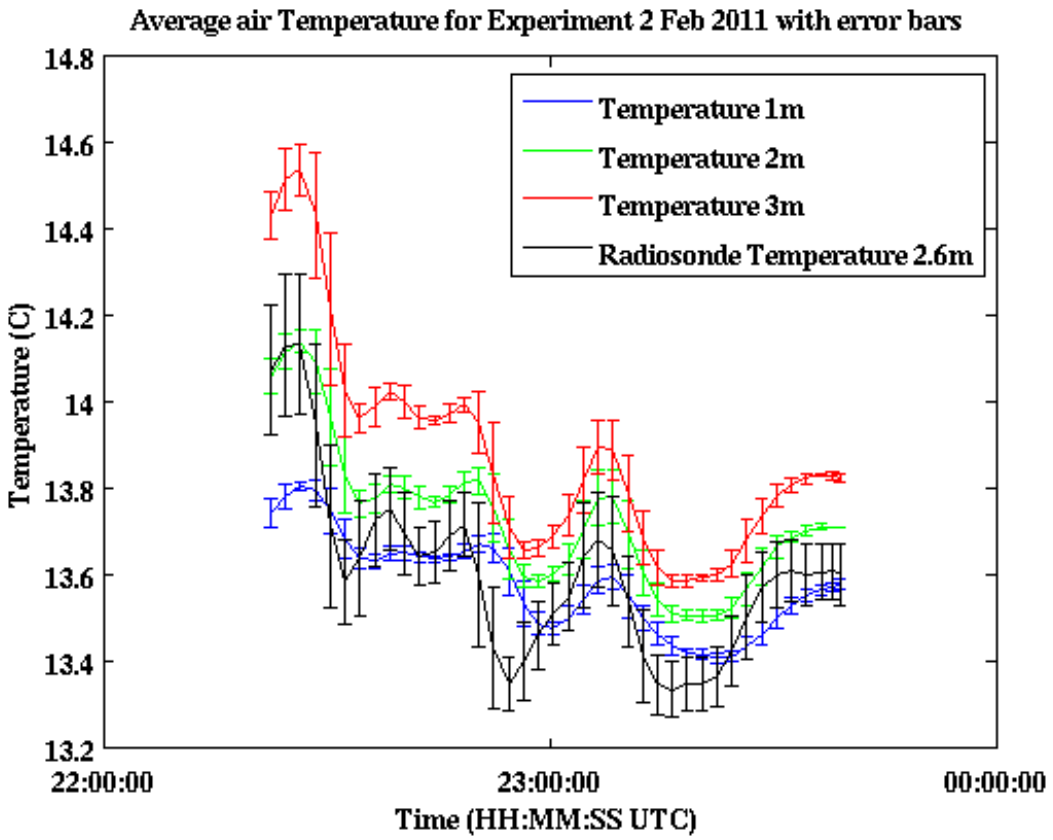

Figure 8. Vertical variation and error range for temperature during the deployment on February 2, 2011. The on standard deviation is based on 5-minute averages for each 2-minute period. This as the addition of the radiosonde data in black.

2. Relative Humidity

The relative humidity measurements in Figure 9 from our test experiment show similar properties as the temperature sensors. This intercomparison plot indicates consistency of all three HOBO sensors with similar bias from sensor 2.

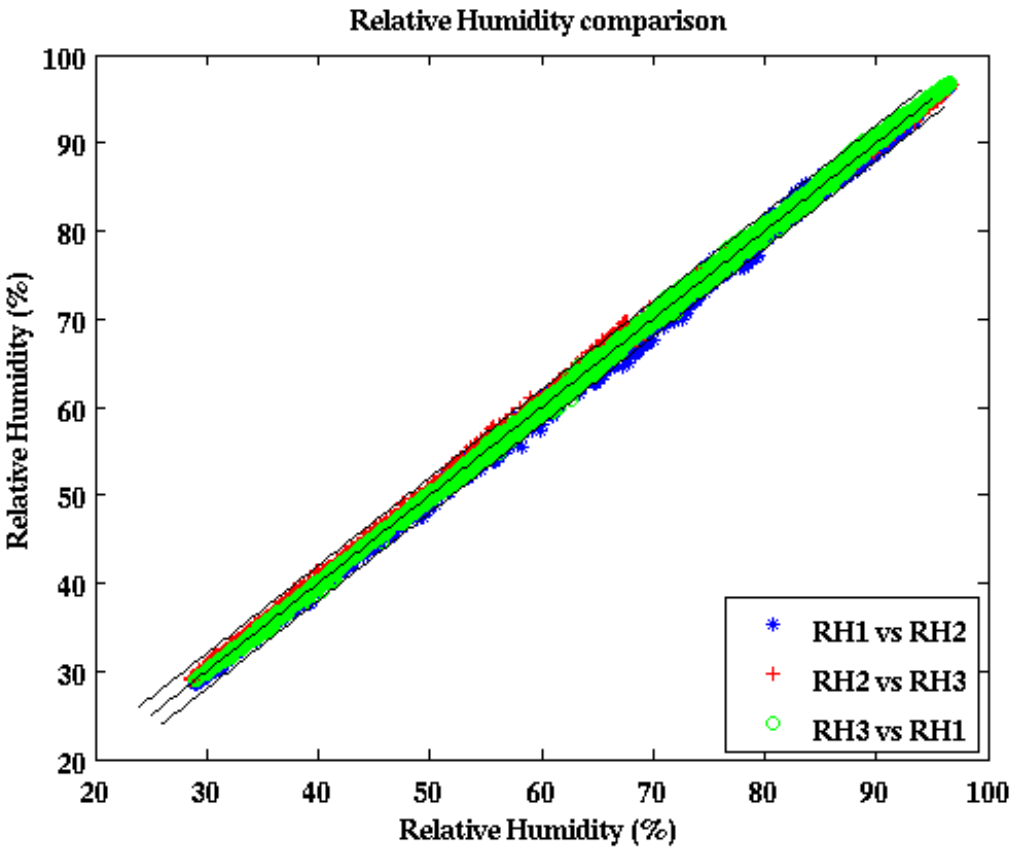

Figure 9. Relative humidity comparison with the three instruments all at the same height. The lines represent a 1 to 1 line with a ± 2% error bar. The relative humidity listed on the left in the legend is plotted on the X axis.

The time series (Figures 10 and 11) show that sensors all respond similarly to variations in relative humidity. There is a slightly low bias toward sensor 2. The statistical significance of the measured relative humidity is shown in Figure 12 using the standard deviation. The error associated with the standard deviation for February 2, 2011 shows relatively small errors in relative humidity measurements. Variations in the radiosonde probe are much higher over the same period of time in Figures 13.

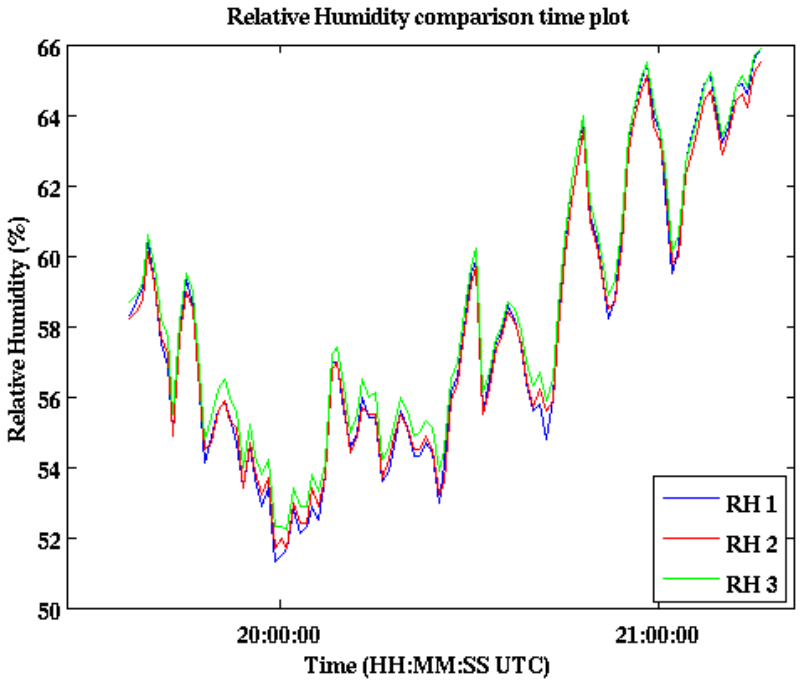

Figure 10. Time series plot of relative humidity during calibration test. This period of 1.5 hours shows movement and differences in measurement.

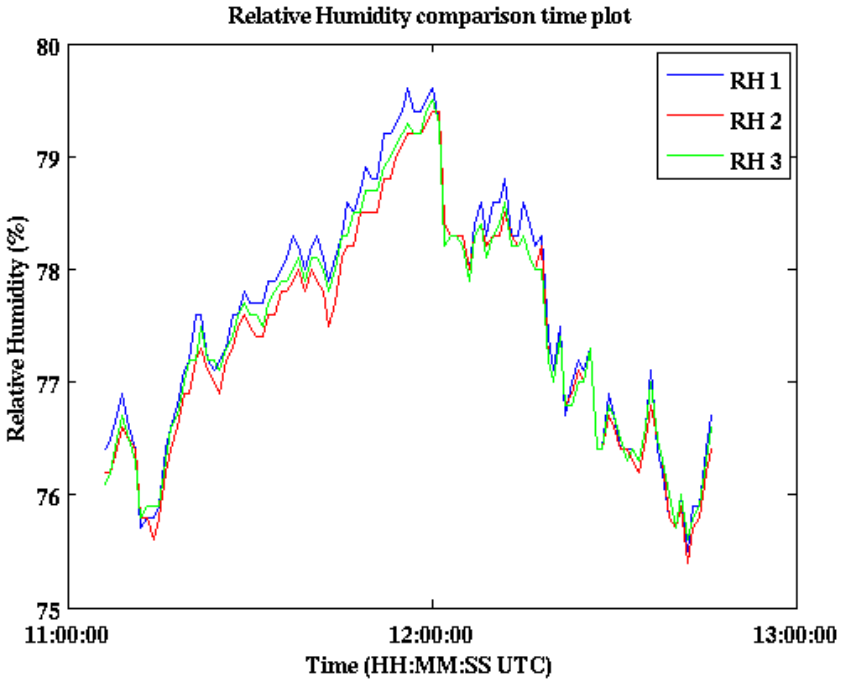

Figure 11. Time series plot of relative humidity during calibration test. This period of 1.5 hours shows movement and differences in measurement.

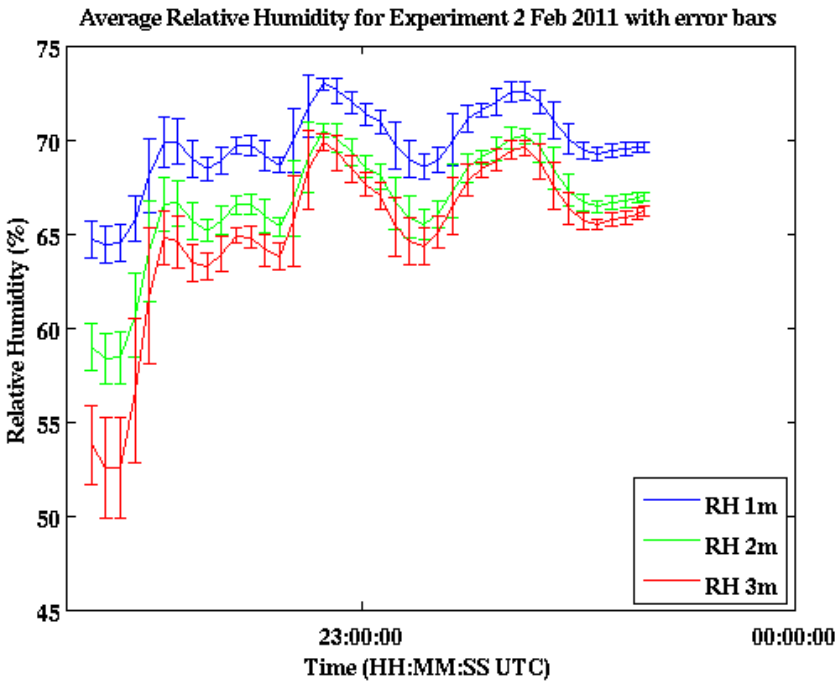

Figure 12. Error plot of relative humidity with 5-minute averages and the standard deviation stepped every 2-minutes. This plot for the data from February 2, 2011.

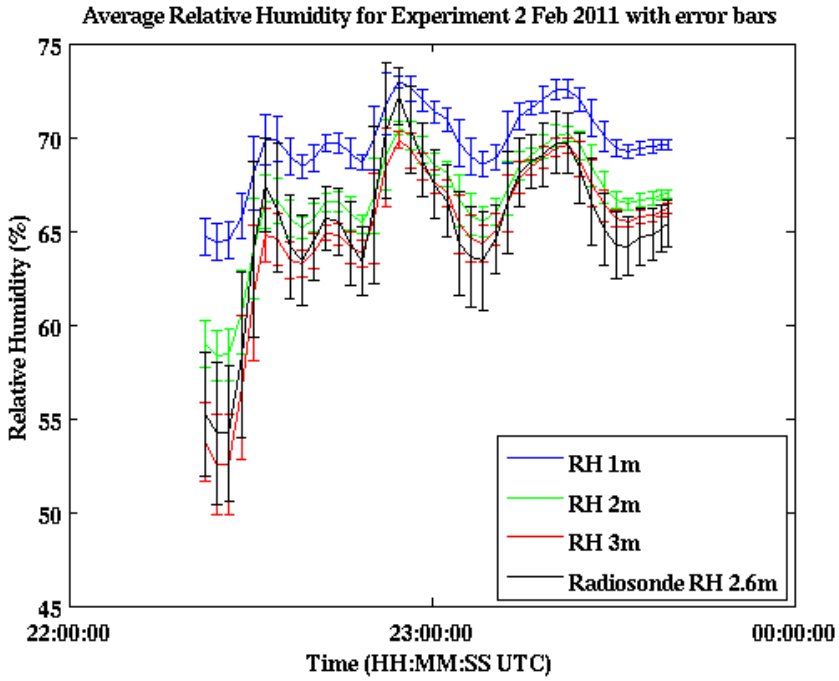

Figure 13. Relative Humidity error based the standard deviation on 5-minute averages every two minutes. This plot is for the data from February 2, 2011.

3. GPS

Small and inexpensive GPS receivers were installed on small buoys that were subsequently tested against various other wave-measuring buoys during the HiRes2010 experiment by Prof. T. Herbers' group (Herbers et al. 2011). The same GPS receiver set was attached to the MOAS to test whether the spar buoy could also be used to characterize the surface waves. Our GPS data are similar to that measured by the same device attached to the Datawell buoy (Figure 14) and similar to the Datawell data. The peak near 0.08 Hz represents long period swell energy. We see that the energy is similar for each measurement near the long period swell. The source of the peak at very low frequencies for the GT31 is unclear and not related to the surface gravity wave field. This error is present in all of the GT31 GPS units. This longer period energy or noise that is filtered out in the Datawell data stream using a 0.01 Hz high-pass filter. The GT31 does not resolve energy beyond 0.5 Hz. Calculations of significant wave height were done on both the full energy spectrum and the area associated with dominant wind-sea and swell waves of 0.05 – 0.3 Hz (Figures 15–17).

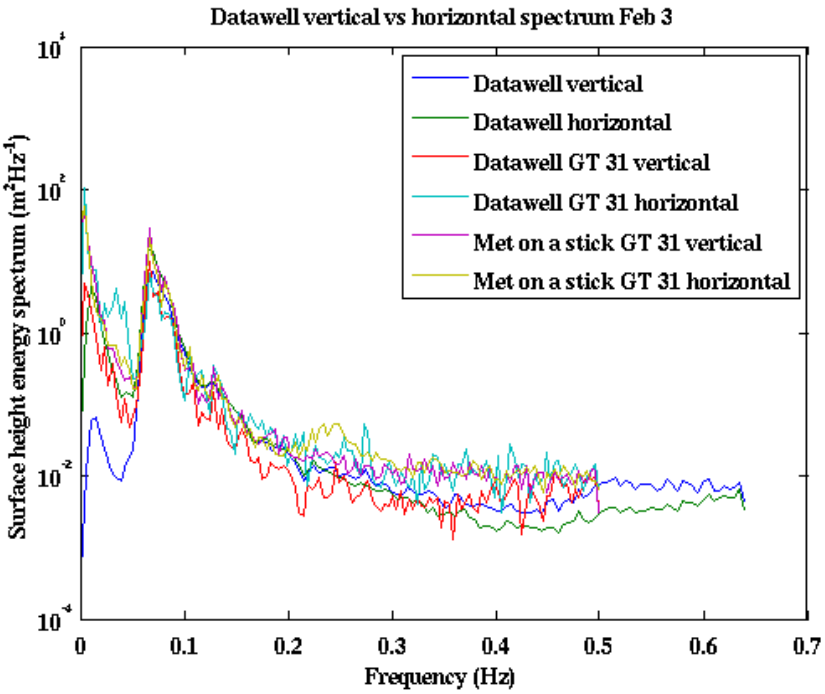

Figure 14. Energy spectrum of GPS GT-31 attached to the Datawell buoy and the MOAS buoy and the NPS Datawell buoy from February 3, 2011

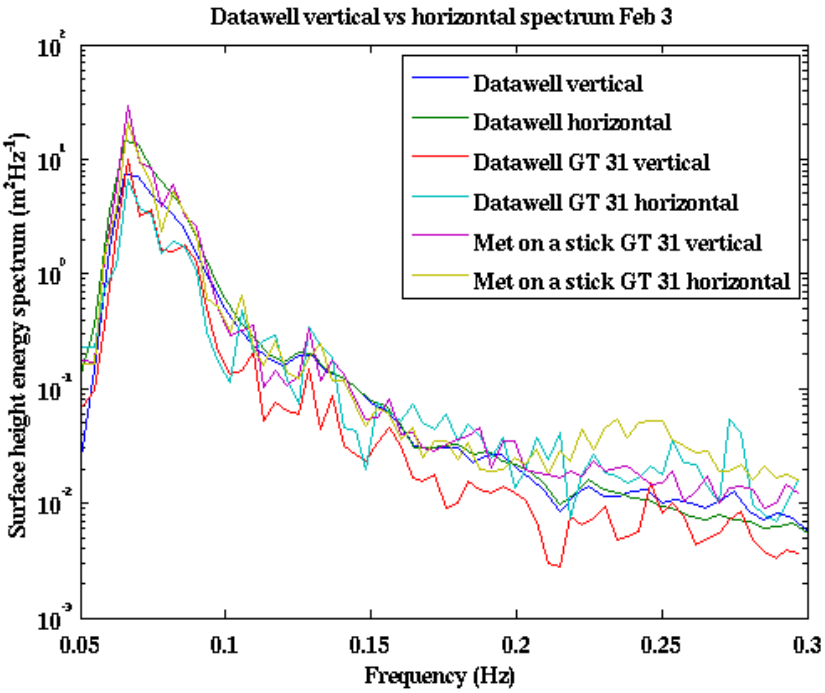

Figure 15. Energy spectrum of GPS GT-31 on the Datawell buoy and the MOAS buoy and the NPS Datawell buoy from February 3 2011. This figure shows a range between 0.05 – 0.3 Hz of the entire spectrum.

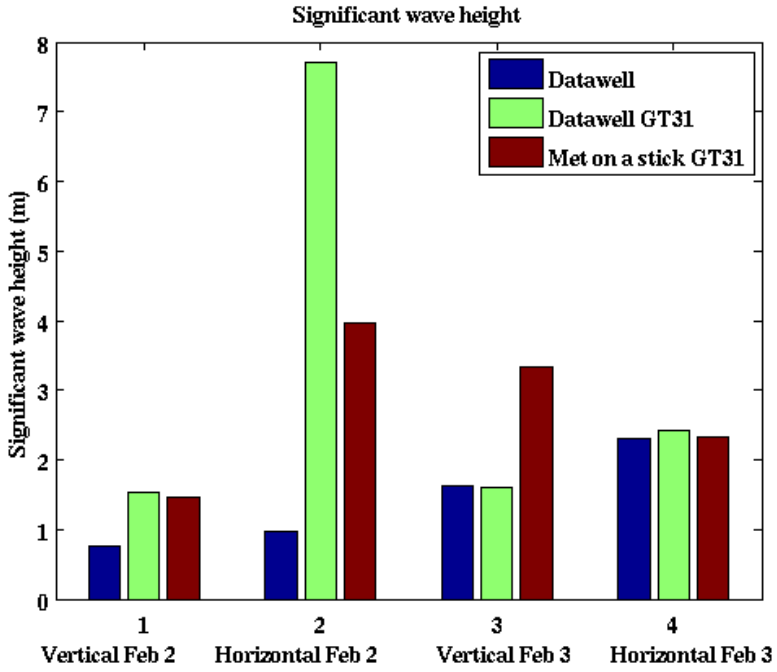

Figure 16. Significant wave height calculated from the entire energy spectrum for both February 2 and 3, 2011.

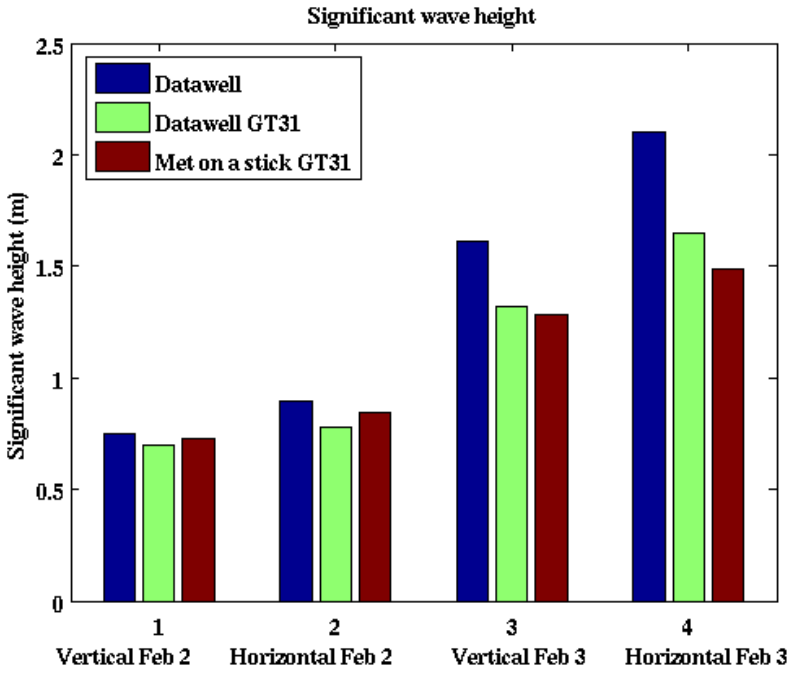

Figure 17. Significant wave height calculated from the 0.05—0.3 Hz part of the energy spectrum for February 2 and 3, 2011.

The vertical energy spectrum from the Datawell buoy is used to calculate significant wave height, which allows us to determine our ability to accurately capture the energy of the waves with the GT31 sensors. The GT31 horizontal energy spectrum is expected to be more accurate and would yield better results for energy spectrum and thus a better calculation of significant wave height.

Herbers et al. (2011) has used the GT31 in deep water with some success. In calculating the significant wave height, they used the more accurate horizontal spectrum, since it has a higher resolution. Using the horizontal spectrum for wave height calculation in shallow water is potentially problematic since a water parcel no longer travels in a circle but in an ellipse, according to linear wave theory (Kinsman 2002 Ch. 3). We calculated significant wave height from both the horizontal and vertical spectra in order to visualize how well the GT31 GPS on the MOAS resolved the energy from the waves. We used the spectra of the Datawell Waverider as the standard for comparison (Herbers et al. 2011). Comparing the significant wave heights calculated on February 2, 2011, there was a 20% increase from the vertical to the horizontal significant wave height

calculated using the Datawell energy spectrum. On February 3, 2011, the corresponding increase was 30%. The depth of the water under the MOAS (Figure 18) is shallow enough that the vertical and horizontal energies are not equal, validating the elliptical motion expected for intermediate water depths. The GT31 fails to capture the magnitude of this difference.

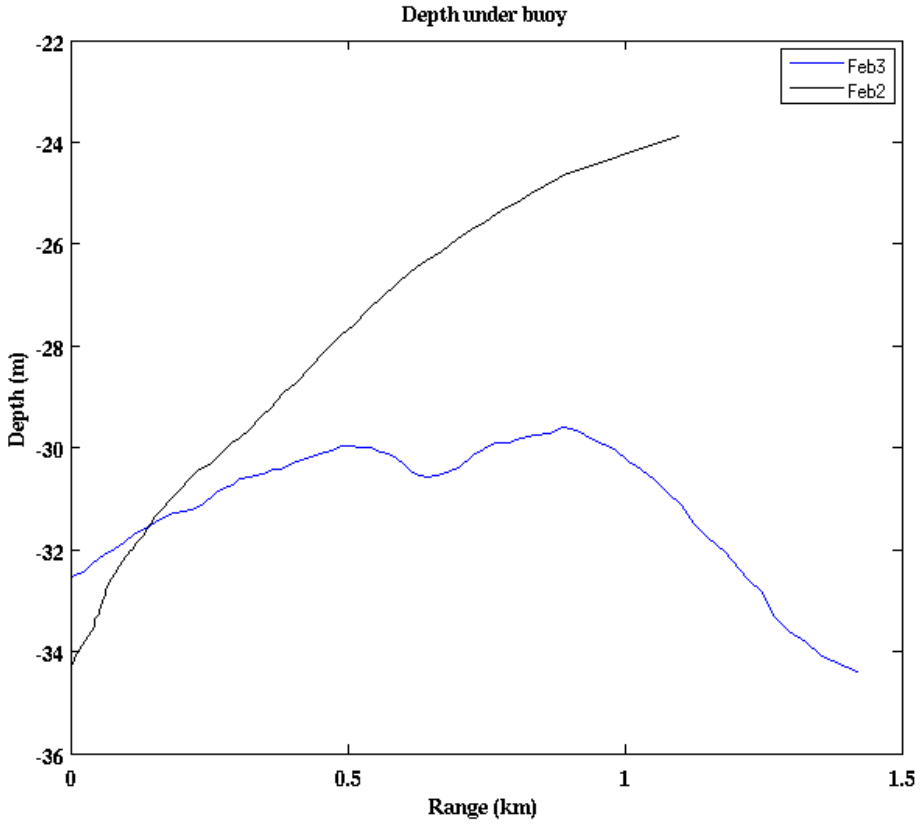

Figure 18. Water depth beneath the MOAS plotted from the initial location during February 2 and 3, 2011 deployments. The horizontal axis shows the range of travel from the initial deployment position. These data are derived from bathymetry of Monterey Bay, and the GPS position.

4. Wind

Wind data shows the structure of the atmosphere. They are reasonably consistent in time and with the different level wind measurements. It has a much wider variability than the temperature or humidity sensors (Figure 19). The gridded appearance of the data shows the impact of the limited resolution wind measurement of the HOBO sensors at

0.38 m s^{-1}. In Figure 20, a time series of the wind measurements from all three levels are compared with their corresponding error bars representing the standard deviation of the measured wind speed. Here we see the average wind speed at 1 meter is higher than that at 2 m. However, the overlap of corresponding error bars suggest little statistical significance of the difference. Hence, due to the limited sensor resolution, this particular set of wind sensors only results in quality data when wind shear at different levels is significant.

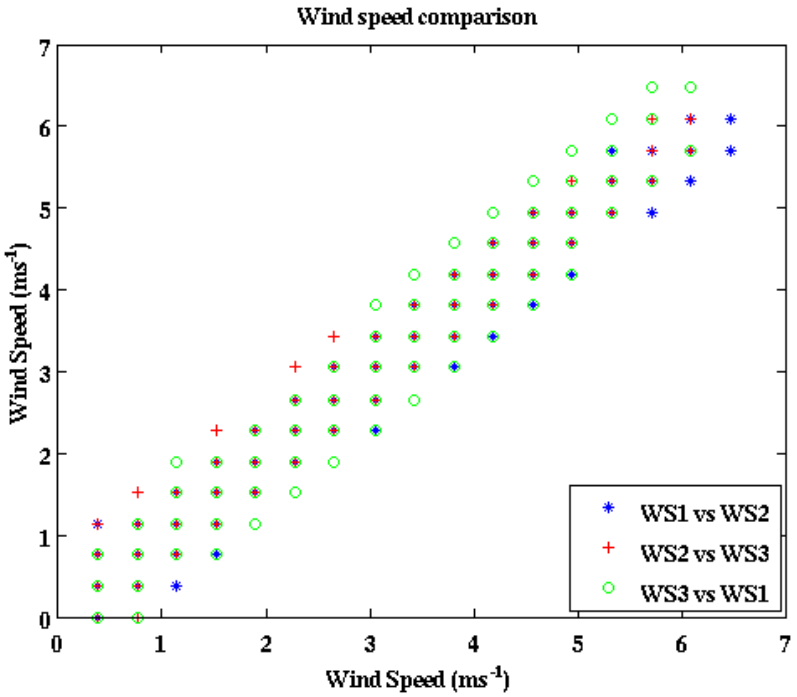

Figure 19. Wind data compared to each other. It is important to note that the variability is 1 m s^{-1}.

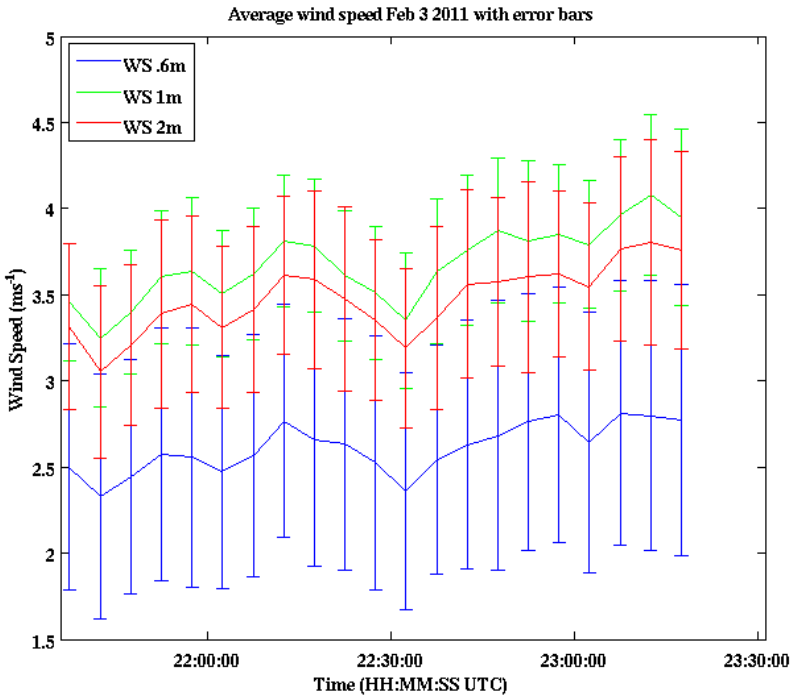

Figure 20. Wind plots from February 3, 2011. Error bars calculated using the standard deviation of the data used to obtain the average wind speed.

III. DATA ANALYSIS

A. DATA OF INTEREST

In this section, we will use some example measurements to illustrate the use of the MOAS measurements for understanding processes occurring at the air-sea interface. The measurements to be discussed will be organized by deployments for each cruise, the June deployment for HiRes2010 cruise on the R/V Sproul, and the January and February deployments on the R/V John H. Martin in conjunction with NPS at-sea classes. Details of each deployment were discussed in Chapter II.

1. June 2010

The June 2010 deployments, using an early version of the MOAS, were in moderate to high wind and rather rough sea state conditions. In spite of the strong wind, the MOAS was able to stay in vertical position, thus able to provide realistic vertical profiles. Figure 21 shows an example of the measured wind speed from the three levels on the MOAS. Here, the decrease in wind speed with descending heights is larger than the sensor resolution and are considered real. The results in Figure 21 indicate a significant decrease in wind speed that would be occurring over the bottom meter above sea level, as the wind speed would need to change from near 7.5 m s^{-1} to zero close to the surface.

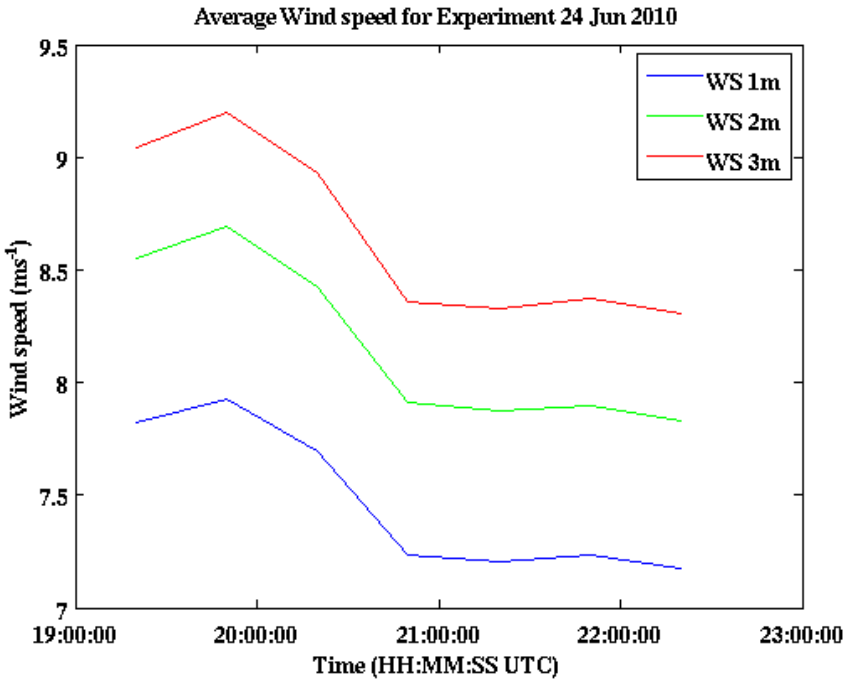

Figure 21. Wind speeds for June 24, 2010, during HiRes2010, plotted as 30-minute running averages.

Temperature in the ocean measured on June 20, 2010, shows us a cold skin temperature (Figure 22). The atmospheric temperature is warmer at 1 meter than any other level (Figure 23) showing that there is some interaction at the interface creating this situation.

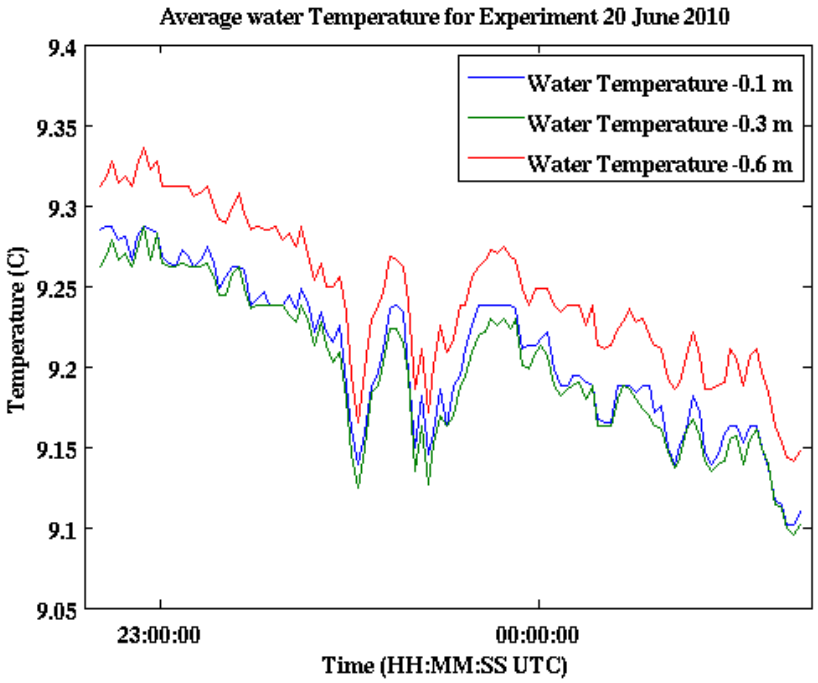

Figure 22. Sea temperatures measured on June 20, 2010, during HiRes2010.

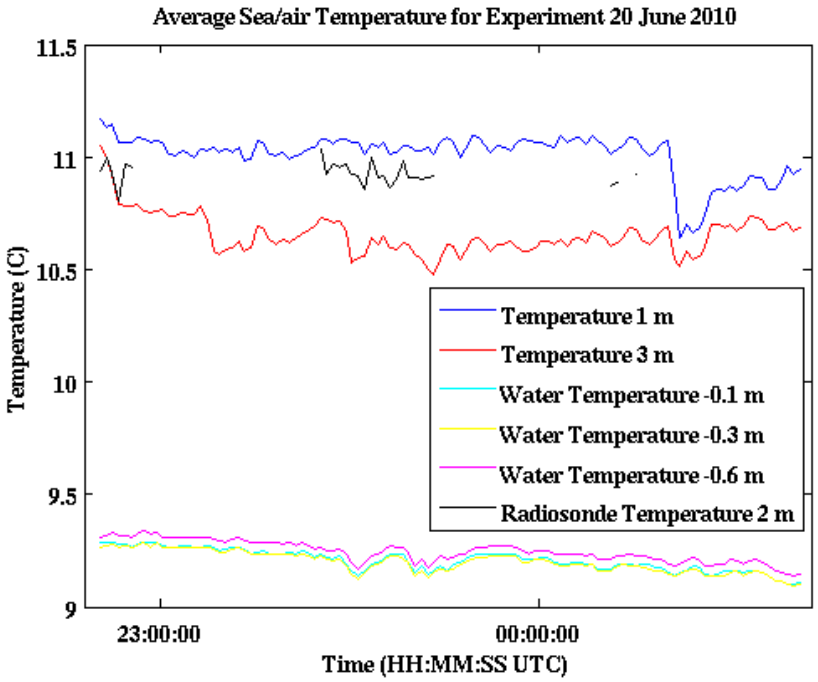

Figure 23. Air/sea temperatures June 20, 2010 during HiRes2010. The radiosonde data is intermittent because the ship was in and out of range.

2. January 2011 Deployment

The deployment in January 2011 gave a good example of the vertical thermal structure and its transition throughout the day (Figure 24). We can see the unstable thermal conditions are present in the morning and the results of daytime heating on both the atmosphere and the surface layers of the water. In Figures 25–27, we have cut this time period into sections to better see the structural changes that take place. The atmosphere takes less than half an hour to become stable after the surface air temperature warms to greater than the water temperature. The water temperature thermal structure does not appear to become stable during this time series even though it shows some significant warming (Figure 28).

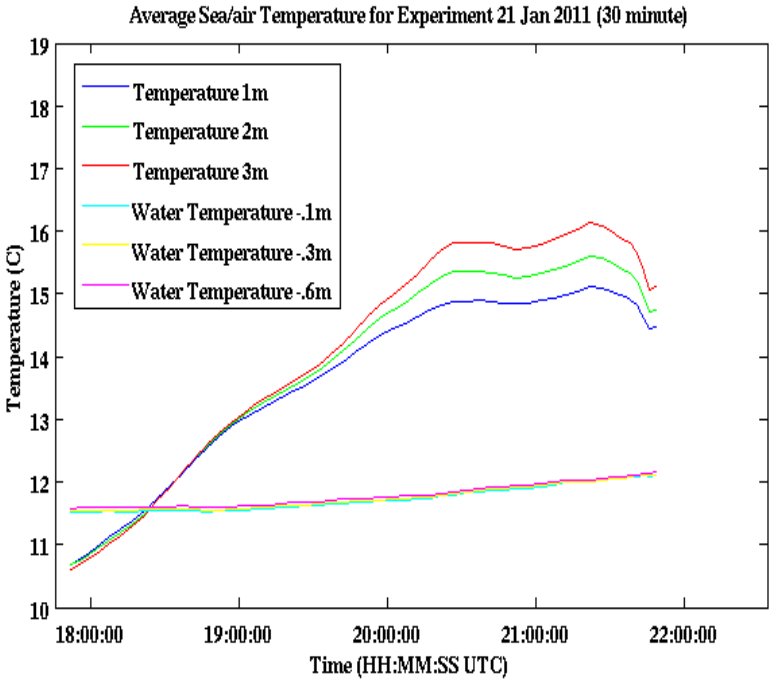

Figure 24. Air/sea temperatures January 21, 2011. The temperatures show the transition from unstable to stable thermal stability.

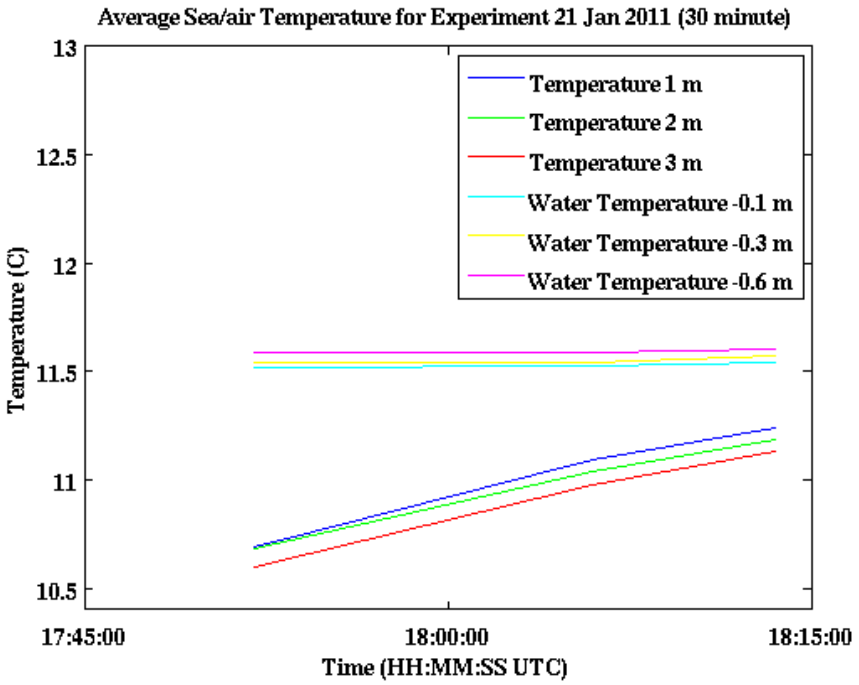

Figure 25. Air/sea temperatures January 21, 2011. This is the thermally unstable period of time.

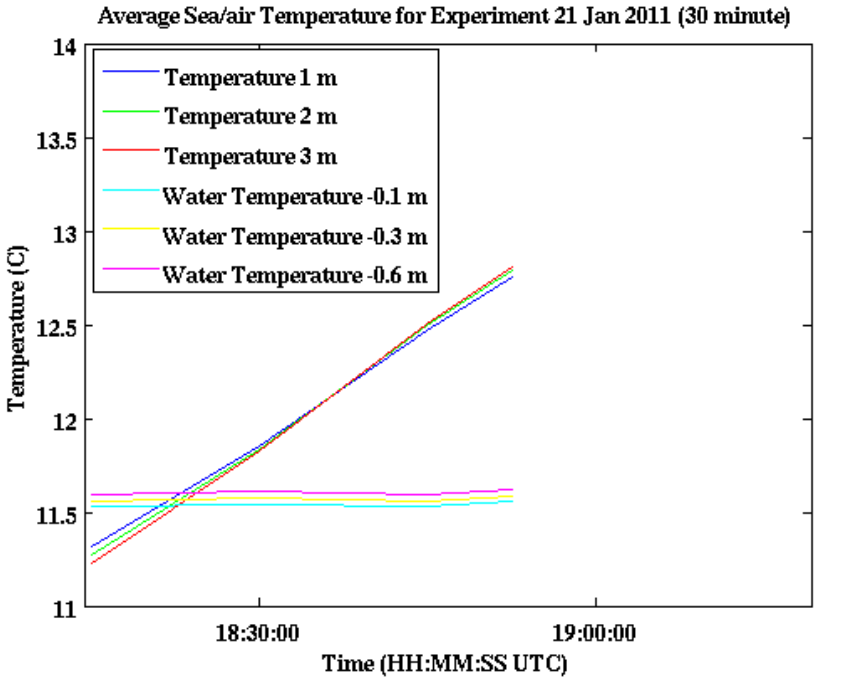

Figure 26. Air/sea temperatures January 21, 2011. Shown here is the transition from thermally unstable to thermally stable stratifications.

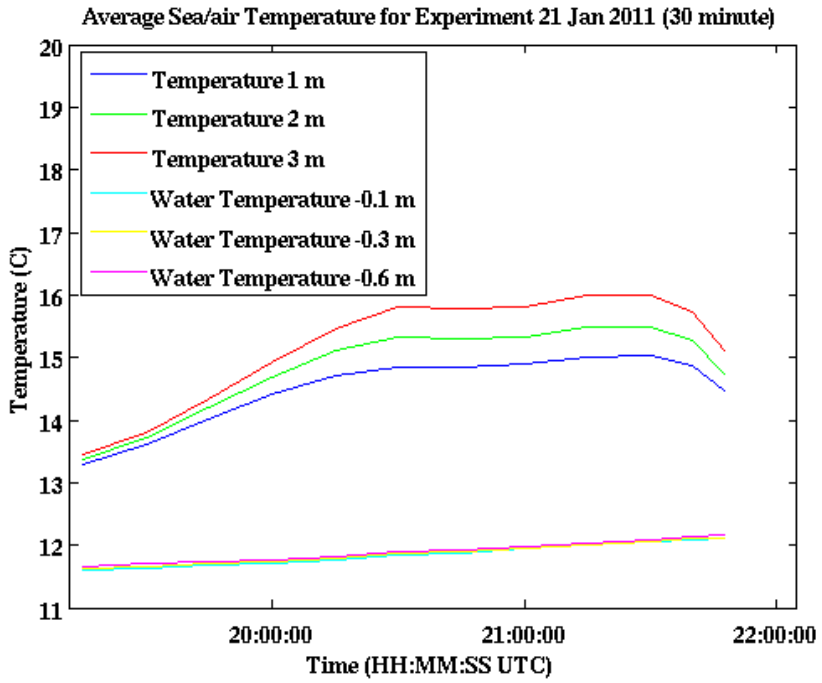

Figure 27. Air/sea temperatures January 21, 2011. The temperatures show thermally stable stratification near the surface.

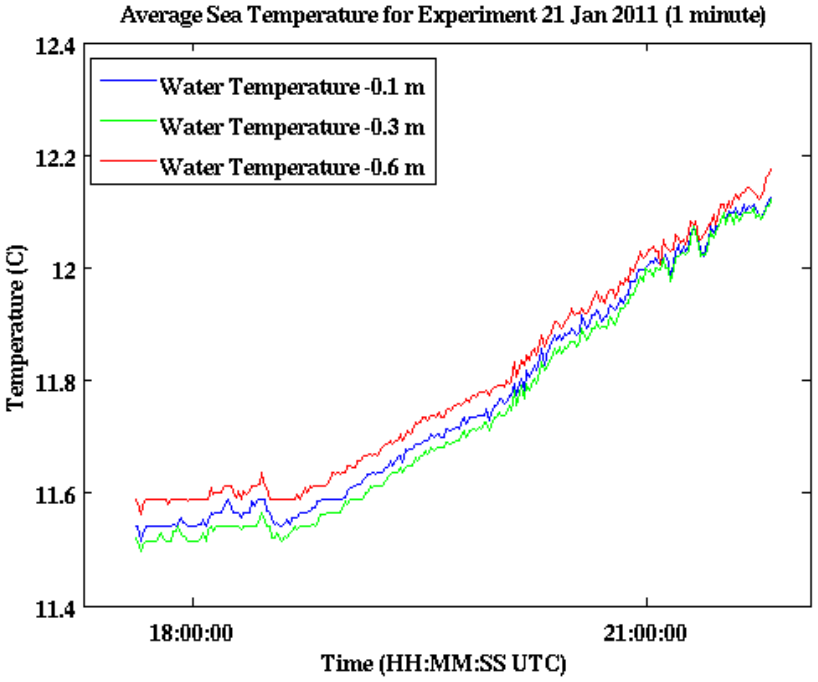

.

Figure 28. Sea temperatures measured on January 21, 2011.

In Figure 29, the measured vertical wind profile is compared to that based on MOS theory and measurements from the upper two levels of measurements on the MOAS. It is seen that the wind at 1 m is less than the value expected from MOS. Hence, the observed near surface shear is larger than what is expected from MOS theory. This result does not seem to be directly related to thermal stability. The profiles on the right are from unstable and neutral conditions, where the values on the left are from more stable conditions, all showing increased shear at the lower levels. Thermal stability profiles indicated by the potential temperature (Figure 30) also show differences with MOS. The neutral conditions follow very well, while the unstable and stable conditions show some deviations from MOS.

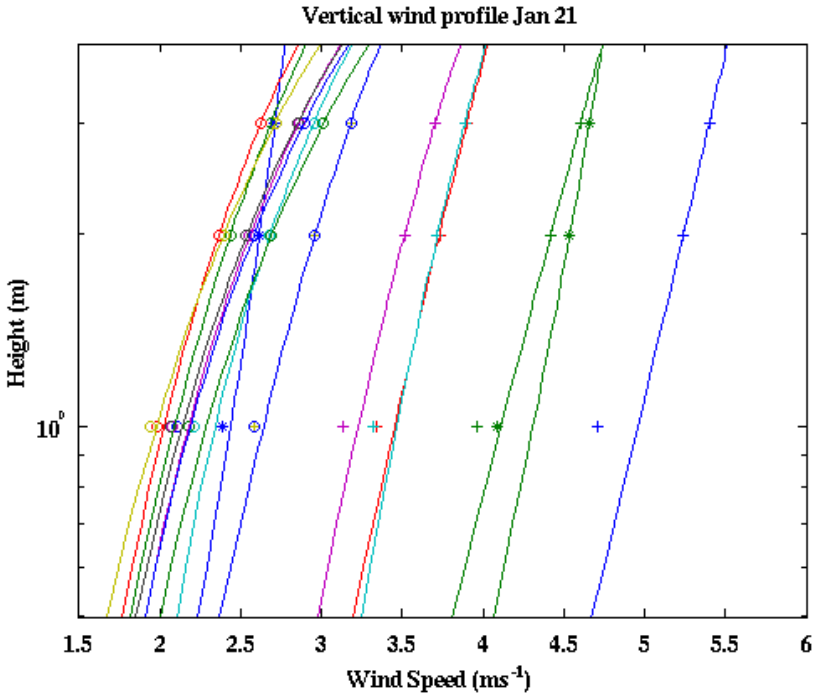

Figure 29. Vertical wind profiles January 21, 2011, that show the calculated MOS profile using the top two of three measured levels. The different symbols showing the measurements at 1, 2, and 3 m correspond to thermally unstable (*), neutral (+), or stable (o).

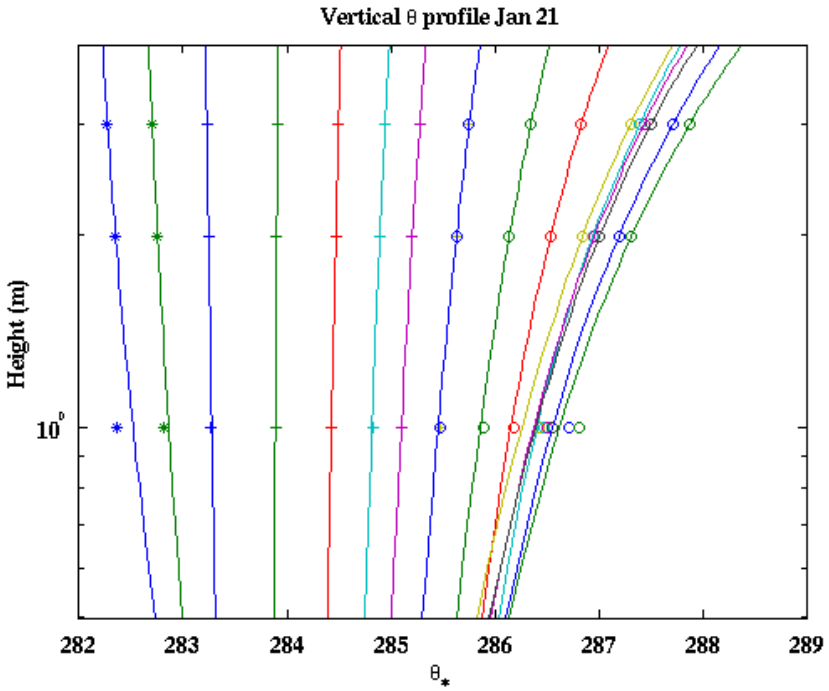

Figure 30. Vertical potential temperature profile from January 21, 2011, calculated using MOS and the upper two measurement levels. The different symbols are used to indicate when the atmosphere is thermally unstable (*), neutral (+), or stable (o).

Relative humidity is a difficult variable to discover what is really happening at the surface. It, nevertheless, indicates how close the air is to saturation, although it does not indicate the amount of moisture in the air. In Figure 31, the relative humidity is compared to the specific humidity. There is some increase in moisture in the atmosphere near the surface during the day, decreasing slightly during the maximum heating period of the day. The relative humidity indicates that the air is not close to saturation as would be expected near the interface of the ocean.

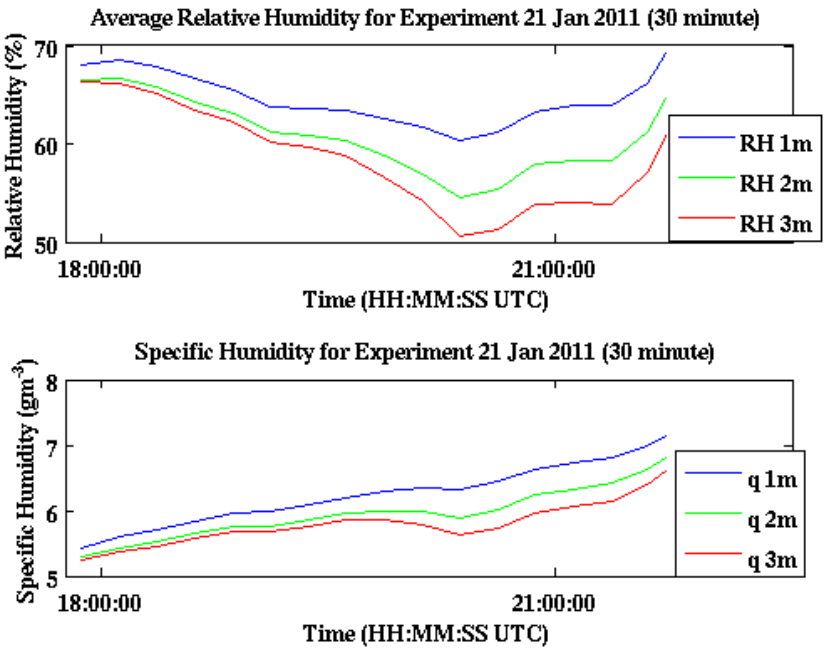

Figure 31. Relative humidity and specific humidity on 21 January 2011.

3. February 2011 Deployments

The wind on February 3, 2011, shows a reversal in direction between 1 and 2 m (Figure 20 and 32). Although the wind speed differences are not statistically significant, there are reasons to believe this is a real phenomenon. This can be seen from comparisons between measurements from February 2 and 3 of 2011. No wind reversal was observed on February 2 (Figure 33). Our observation record indicated significant difference in swell conditions in these two days with bigger swell on February 3. Although there were differences in thermal stability in the lower atmosphere, the difference in swell height is perhaps the dominant difference between the two days. We calculated the vertical wind profiles using MOS from the top and bottom wind levels, which shows this is a significant difference from MOS (Figure 34). The calculation for the 2nd is also shown in Figure 36 where it is still similar to MOS. There is a significant shift in the lowest wind speeds, indicating a more rapid loss of momentum near the surface than expected from MOS. There has been some modeling done on this subject that shows the disruption of the wind and pressure structure when swell is no longer in equilibrium with the wind

(Sullivan et al. 2008, 2010). One of these situations is when the swell is moving faster than the wind, creating surface jets. Any correlation of wind speed to swell would require much higher resolution instrumentation.

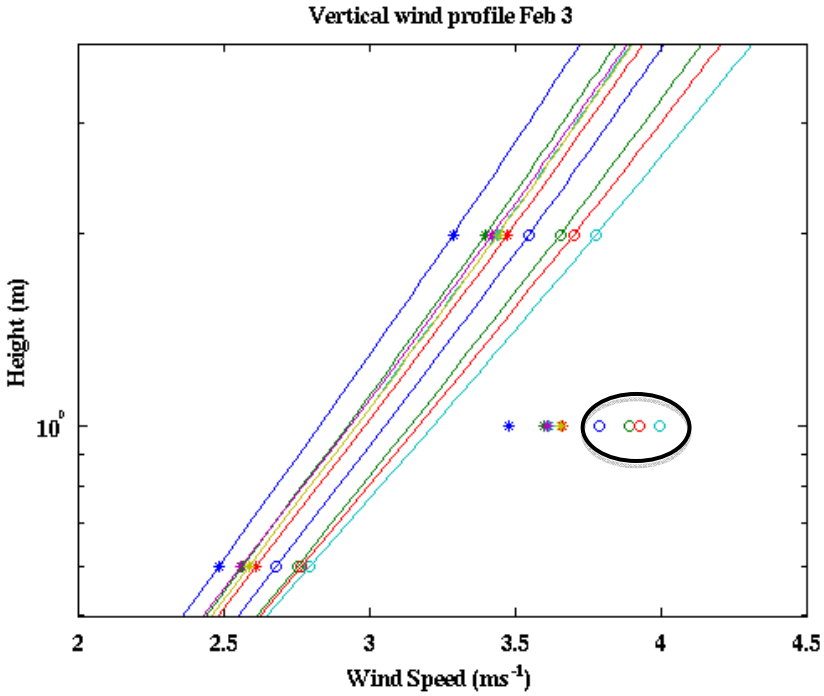

Figure 32. Vertical wind profile on February 3, 2011, showing the calculated MOS profile using the top and bottom of three measured levels (lines) and the measured wind (symbols). Different color/symbols denote results from a different time starting at 2140 and ending at 2320. Each profile represents an average profile from 30 minutes of measurements.

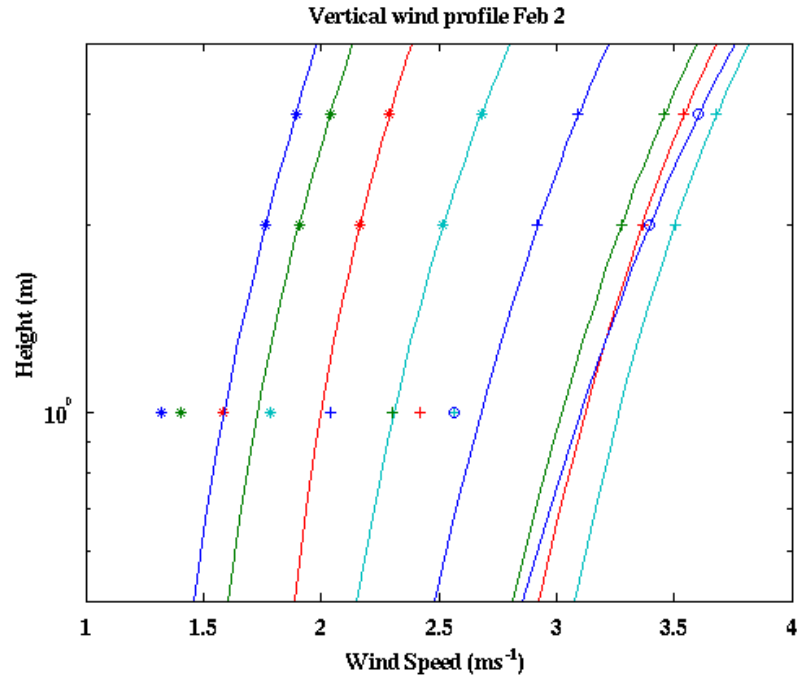

Figure 33. Vertical wind profile on February 2, 2011, showing the calculated MOS profile using the top two of three measured levels (lines) and the measured wind (symbols). Different color/symbols denote results from a different time starting at 2220 and ending at 2340. Each profile represents an average profile from 30 minutes of measurements.

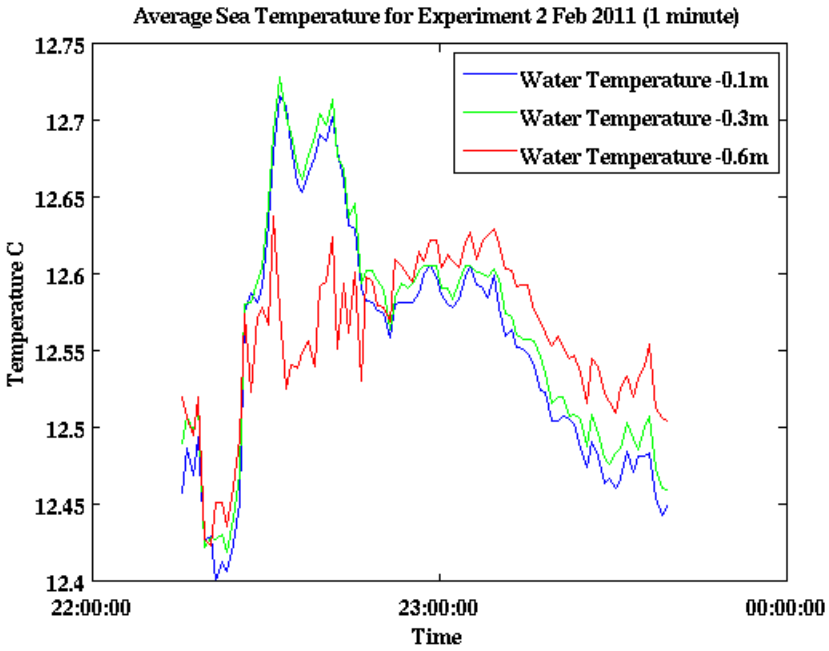

Figure 34. Sea Temperatures averaged over one minute for February 2, 2011.

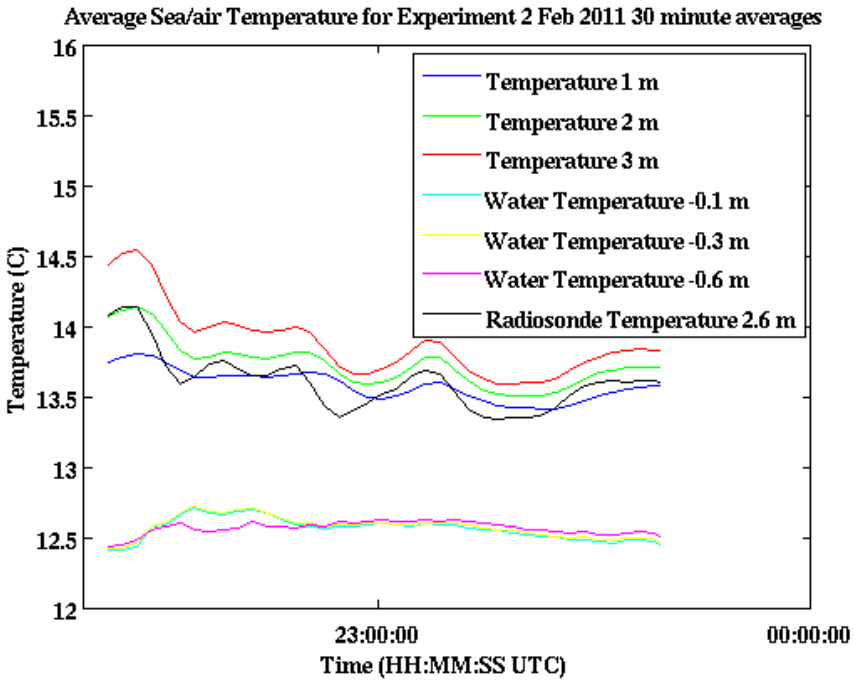

Figure 35. Temperature averaged over thirty minutes for February 2, 2011.

The sea temperature measurements indicate that the MOAS may drift through rather different water properties (Figure 34). Here we can see as the buoy is drifting it encounters some warm pool of water resulting in significant changes in water temperatures over a short period of time. There is an inversion in the water temperatures with the cooler water on top (Figure 35). There is further evidence that this is a common occurrence from Fairall, et al. (1996) and Figures 36 and 37 showing similar measurements made in the same region on February 3.

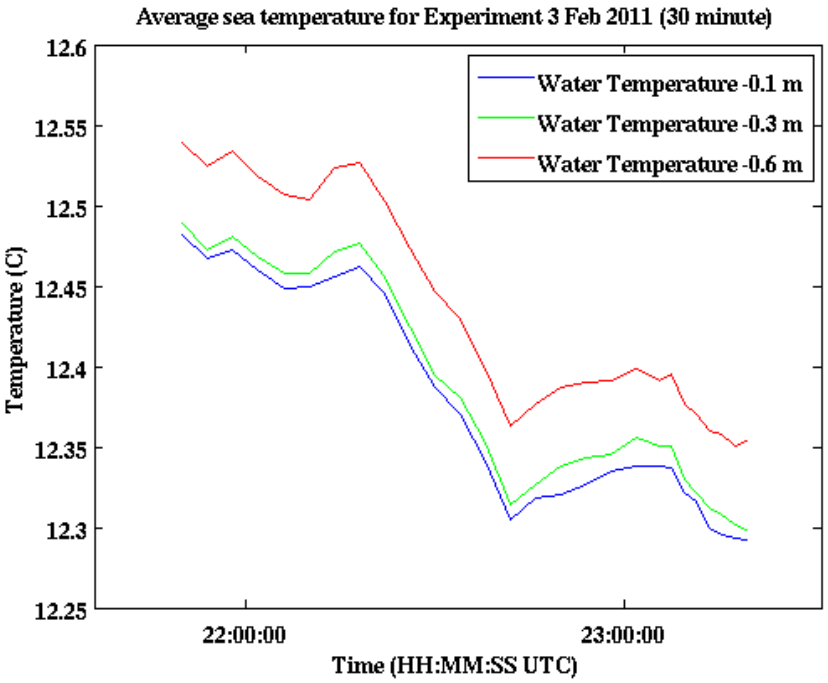

Figure 36. Sea temperatures averaged over 30 minutes on February 3, 2011.

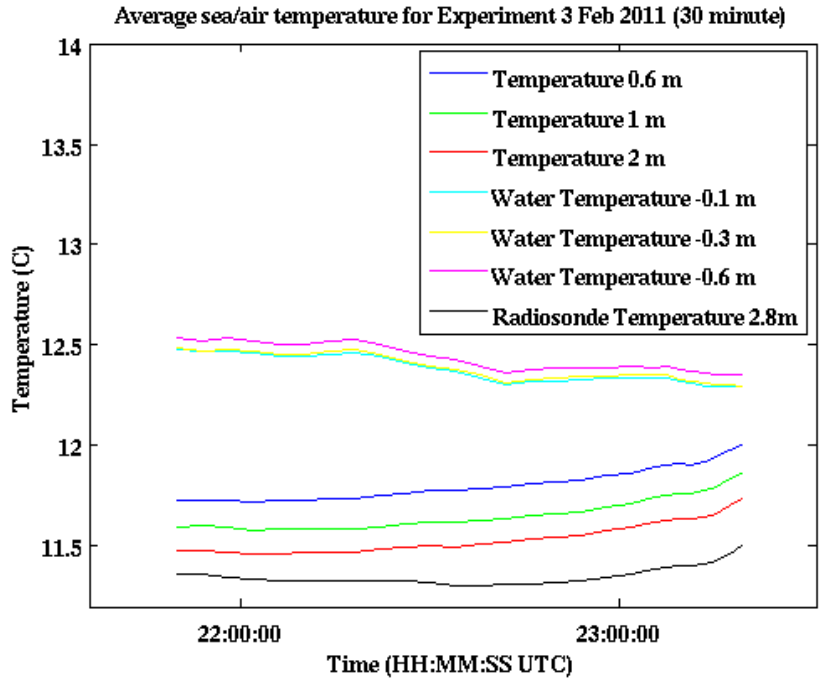

Figure 37. Temperatures measured on February 3, 2011, showing a complete inversion of temperatures through the water and atmospheric layers.

4. Flux Calculation

Using MOS theory we calculated the surface flux of momentum, latent heat, and sensible heat (Figures 38–40). These fluxes are within expected ranges for this level of the atmosphere. The sensible heat flux shows the transition between the unstable atmosphere and the stable atmosphere with the daytime heating. We calculated these values for Feb. 2, but the difference in the wind from one level to another is so small that the resolution of the instruments calls into question the validity of the data. For Hi-Res dates, we do not have sufficient data, and for February 3, the wind reversal does not allow use of MOS theory.

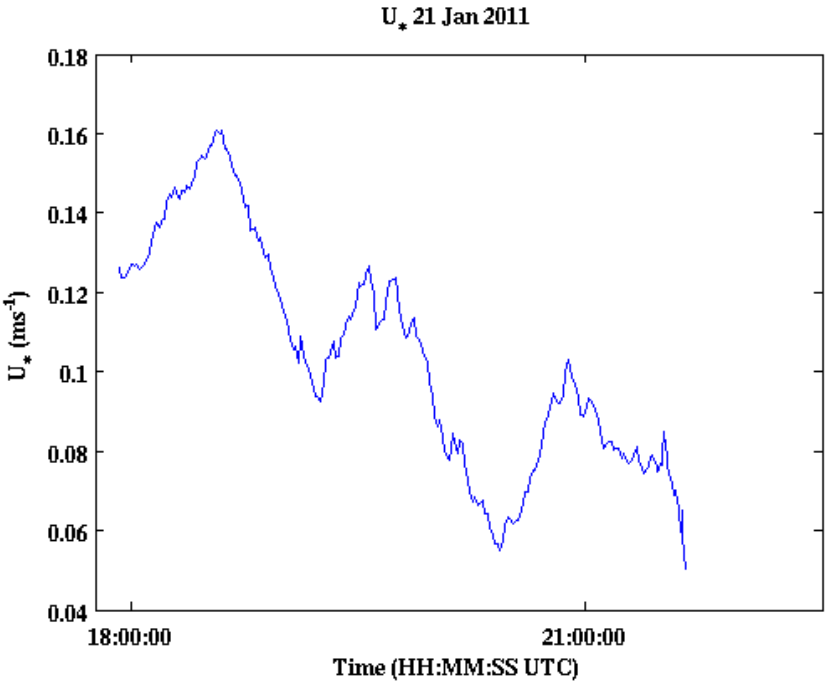

Figure 38. Momentum flux calculated from data on January 21, 2011, using the top two levels of measurement.

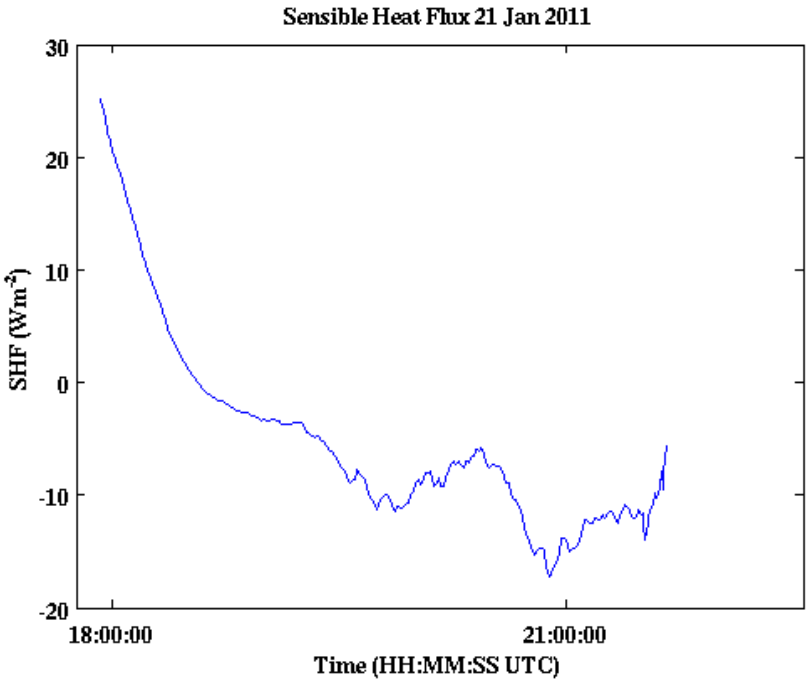

Figure 39. Sensible heat flux (SHF) calculated from data on January 21, 2011, using the top two levels of measurement.

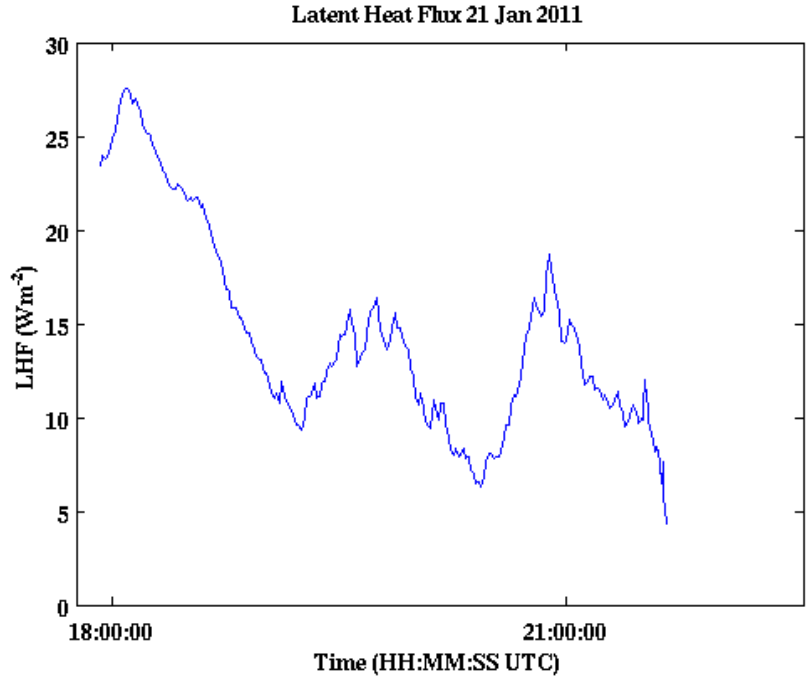

Figure 40. Latent heat flux (LHF) calculated from data on January 21, 2011, using the top two levels of measurement.

THIS PAGE INTENTIONALLY LEFT BLANK

IV. CONCLUSIONS AND RECOMMENDATIONS

A. SUMMARY

This thesis work documented the design, instrumentation, and deployment of the NPS met-on-a-stick, or the MOAS, and made initial analyses of the MOAS data to examine data quality and the potential use of the MOAS in characterizing the atmosphere and the upper-ocean near the air-sea interface. The MOAS has gone through several phases from the Hi-Res2009 experiment in June 2009 to the final testing on the R/V John H. Martin on Feb. 2011. The latest version was tested in February 2011 during the at-sea class and shows that the MOAS is able to stay upright in weak to moderate wind conditions.

The objective of data analyses in this thesis is to evaluate the sensor performance and to evaluate the adequacy of the MOAS measurements for more in-depth air-sea research studies. We found that the instruments at different heights resemble each other to a certain degree. In case of the wind data, the consistency of the sensors is limited due to the coarse resolution of the HOBO wind sensors, although the temperature and humidity sensors show reasonable agreement. A GPS navigator, GTS 31, was attached to the buoy for wave height measurements. In comparison with the Datawell accelerometer wave measurements, it was found that the performance between the GTS 31 sensors attached onto the Datawell buoy gave very similar results to those from the GTS 31 attached to the MOAS. This suggests that the uncertainty in the MOAS wave measurements is introduced by the quality of the GPS signal, not the platform, which gave us the confidence of application of the MOAS for wave measurement.

Examples of the MOAS measurements were given to examine the ability of the MOAS in quantifying the near surface vertical variations of wind and thermodynamic variables. In one case, the MOAS measurements revealed the development of the atmospheric boundary layer in response to thermal stability change represented by air-sea temperature difference. In several deployments, we observed cooler temperature near the surface compared to those at less than 1 meter depth. These findings are consistent with

the cool skin effect. In examining the measured vertical wind, and temperature profiles and compared to those predicted using MOS theory and two levels of measurements, we found frequent deviation from the MOS theory at the low levels. In one case with high seas of swell, the second lowest level actually sampled maximum wind speed compared to the altitude above and below. This 'wind reversal' is likely associated with effects of fast moving swell that actually transfers momentum from the ocean surface to the lower atmosphere. All these examples point to the significant role the MOAS can play in future air-sea study near the interface.

B. RECOMMENDATIONS FOR FUTURE IMPROVEMENTS

The MOAS worked well to gather the data expected. It was reasonably easy to deploy and retrieve, although harder in higher seas conditions with the moving platform. It was also easy to set up and retrieve data. We received good data from all sources based on the platform that we were attached to and the capabilities of the instruments.

The MOAS can benefit from several improvements derived from this thesis study. The wind and GPS resolution is poor, and would need to be improved. The wind instrument is the biggest problem with such poor resolution. It worked well within constraints of its resolution, so the buoy works as a platform for measuring winds. The GPS needs better antenna in order to get rid of the noise in the higher frequencies and the errors in the low frequencies. Dual band GPS would also help eliminate the noise associated with the GPS signal. A better antenna could be placed at the top of the pole to eliminate any interference from the rest of the instruments. The buoy still shows similar measurements to the smaller Datawell buoy, making the platform good for doing wave measurements. Wave measurements could also be done using accelerometers, which could yield better results.

The overall instrument package could be improved with more accuracy and greater resolution, both in sampling and time response. Many of these more accurate and better resolution instruments have greater power requirements (and costs) or could be more difficult to interface with. Care should be taken in choosing instruments for the next generation to ensure the instruments are self-contained and deployable by two people.

This platforms instrumentation could be expanded or changed to include many different kinds of instruments increasing its capacity and usefulness. It could become a great asset to research that requires more accurate information at the air sea interface, and would be able to unlock the mysteries of this important region for better modeling and understanding.

THIS PAGE INTENTIONALLY LEFT BLANK

LIST OF REFERENCES

Businger, J. A., J. C., Wyngaard, Y. Izumi, and E. F. Bradley, 1971: Flux-Profile Relationships in the Atmospheric Surface Layer. *Journal of the Atmospheric Sciences*, **28**, 181–189.

Charnock, H., 1955: Wind stress on a water surface. *Quart. J. Roy. Meteor. Soc.*, **81,** 639–640.

Edson, J., T. Crawford, J. Crescenti, T. Farrar, N. Frew, G. Gerbi, A. Plueddemann, J. Trowbridge, R. Weller, A. J. Williams, C. Helmis, T. Hristov, L. Shen, D. Khelif, A. Jessup, H. Jonsson, M. Li, L. Mahrt, E. Skyllingstad, D. Vickers, W. McGillis, C. Zappa, T. Stanton, Q. Wang, P. Sullivan, J. Sun, S. Wang, J. Wilkin, and D. K. P. Yue, 2007: The Coupled Boundary Layers and Air-sea Transfer Experiment in Low Winds *Bull.Am.Meteorol.Soc.,* **88**, 341–356.

Fairall, C.W., Bradley, E. F., Hare, J. E., Grachev, A. A., Edson, J. B., 2003: Bulk Parameterization of Air-sea Fluxes: Updates and Verification for the COARE Algorithm. *J. Climate,* **16**, 571–591.

Fairall, C. W., E. F. Bradley, J. S. Godfrey, G. A. Wick, J. B. Edson, and G. S. Young, 1996: Cool-skin and warm-layer effects on sea surface temperature. *Journal of Geophysical Research,* **101**, 1295–1308.

Garratt, J. R., 1992: *The atmospheric boundary layer.* New York, NY, Press Syndicate of the University of Cambridge, 316 pp.

Geernaert, G., 2010: Normalizing Air-sea Flux Coefficients for Horizontal Homogeneity, Stationarity, and Neutral Stratification. *J.Phys.Oceanogr.,* **40**, 2148–2158

Gerbi, G., J. Trowbridge, J. Edson, A. Plueddemann, E. Terray, and J. Fredericks, 2008: Measurements of Momentum and Heat Transfer across the Air-Sea Interface. *J.Phys.Oceanogr.,* **38**, 1054–1072.

Graber, H. C., E. A. Terray, M. A. Donelan, W. M. Drennan, J. C. Van Leer, and D. B. Peters, 1999: ASIS—A New Air-sea Interaction Spar Buoy: Design and Performance at Sea. *Journal of Atmospheric and Oceanic Technology,* **17**, 708–720.

Herbers, T. H. C., Jessen, P.F., Janssen, T. T., Colbert, D. B., MacMahan, J. H., 2011: Observing Ocean Surface Waves with GPS-Tracked Buoys. *Journal of Atmospheric and Oceanic Technology,* in review.

Jones, I. S. F., Toba, Y., 2001: *Wind Stress Over the Ocean*, New York, NY, Cambridge University Press, 307 pp.

Kinsman, B., 2002: *Wind Waves: Their Generation and Propagation on the Ocean Surface (Dover Phoenix Editions)*, Mineola, NY, Dover Pubns, 676 pp.

Locosys, 2009: Locosys Technology. [Available online at http://www.locosystech.com/product.php?id=30&zln=en].

Locosys Technology, 2007: GT-31 Specifications. [Available online at http://www.locosystech.com/support.php?zln=en&DL=1&model=GT-31/BGT-31].

MIcroDAQ.com, 2011: 12-bit Temperature/RH Smart Sensor (2m cable) - S-THB-M002. [Available online at http://www.onsetcomp.com/products/sensors/s-thb-m002].

MicroDAQ.com, 2011: HOBO Wind Speed Smart Sensor. [Available online at http://www.microdaq.com/occ/hws/windsp.php].

MicroDAQ.com, 2011: S-TMB-M002 - 12-Bit Temperature Smart Sensor. [Available online at http://www.microdaq.com/occ/hws/temp12.php].

Miller, S. D., 1998: The structure of turbulent and wave-induced wind fields over open-ocean waves, Ph.D thesis, University of California, 221 pp.

National Oceanic and Atmospheric Administration, NDBC - Frequently Asked Questions [Available online at http://www.ndbc.noaa.gov/bht.shtml].

Onset, 2011: HOBO H22 Energy Logger. [Available online at http://www.onsetcomp.com/products/data-loggers/h22–001].

Onset, 2011: Wind Speed Smart Sensor with 3m cable. [Available online at http://www.onsetcomp.com/products/sensors/s-wsa-m003].

Pascal, R. W., M. J. Yelland, M. A. Srokosz, B. I. Moat, E. M. Waugh, D. H. Comben, A. G. Cansdale, M. C. Hartman, D. G. H. Coles, P. Chang Hsueh, and T. G. Leighton, 2011: A Spar Buoy for High-Frequency Wave Measurements and Detection of Wave Breaking in the Open Ocean. *J.Atmos.Ocean.Technol.,* **28**, 590–605.

Rutgersson, A., A. S. Smedman, and U. Högström, 2001: Use of conventional stability parameters during swell. *Journal of Geophysical Research,* **106**, 27,117–27,134,

Smedman, A., U. Högström, H. Bergström, A. Rutgersson, K. K. Kahma, and H. Pettersson, 1999: A case study of air-sea interaction during swell conditions. *J.Geophys.Res.,* **104**, 1054–1072.

Stull, R. B., 1988: *An Introduction to Boundary Layer Meteorology*. Dordrecht, The Netherlands, Kluwer Academic Publishers, 666 pp.

Sullivan, P. P., J. B. Edson, T. Hristov, and J. C. McWilliams, 2008: Large-Eddy Simulations and Observations of Atmospheric Marine Boundary Layers above Nonequilibrium Surface Waves. *J.Atmos.Sci.*, **65**, 1225–1245.

Sullivan, P. P., J. C. McWilliams, 2010: Dynamics of Winds and Currents Coupled to Surface Waves. *Annu.Rev.Fluid Mech.*, **42**, 19–42.

Sullivan, P. P., J. C. McWilliams, and T. Hristov, 2010: A Large Eddy Simulation Model of High Wind Marine Boundary Layers above a Spectrum of Resolved Moving Waves. *Proc. 19th Conference Boundary layer and Turbulence, Keystone, Colorado.*

SX Blue GPS Series, SBAS Made Easy. [Available online at http://www.sxbluegps.com/sbas-made-easy.html].

Vaisala, 2011: Vaisala Radiosonde RS92 - Vaisala. [Available online at http://www.vaisala.com/en/meteorology/products/soundingsystemsandradiosondes/radiosondes/Pages/RS92.aspx].

Vaisala Upper Air. Hydrometeoindustry.org, 2011: [Available online at http://www.hydrometeoindustry.org/catalogue/ProductSheets/Vaisala/UpperAir/VaisalaUpperAirSheet.htm].

THIS PAGE INTENTIONALLY LEFT BLANK

INITIAL DISTRIBUTION LIST

1. Defense Technical Information Center
   Ft. Belvoir, Virginia

2. Dudley Knox Library
   Naval Postgraduate School
   Monterey, California